ZBTB18 interacts with CTBP2 and represses SREBP genes to inhibit fatty acid synthesis in glioblastoma

Ferrarese R.[1§], Izzo A.[1§], Andrieux G.[2,3§], Lagies S[4,5,6], Masilamani A.P.[1], Schulzki R.[1], Shuai Y[1]., Kling E.[1], Ribecco V.[1], Wasilenko A.[1], Heiland D.H.[1], Prinz M.[7,8,9], Kammerer B.[4,5,10], Börries M.[2,3] and Carro M.S.[1*]

[1]Department of Neurosurgery, Faculty of Medicine Freiburg, D-79106 Freiburg, Germany.

[2]Institute of Medical Bioinformatics and Systems Medicine, University Medical Center Freiburg, Faculty of Medicine, University of Freiburg, Freiburg, Germany.

[3]German Cancer Consortium (DKTK), partner site Freiburg; and German Cancer Research Center (DKFZ), Heidelberg, Germany.

[4]Center for Biological Systems Analysis, University of Freiburg.

[5]Spemann Graduate School of Biology and Medicine (SGBM), University of Freiburg, 79104 Freiburg, Germany

[6]Faculty of Biology, University of Freiburg, 79104 Freiburg, Germany

[7]Institute of Neuropathology, Medical Center - University of Freiburg,

[8]Signaling Research Centres BIOSS and CIBSS, University of Freiburg, Germany

[9]Center for NeuroModulation (NeuroModul), University of Freiburg, Freiburg, Germany

[10]BIOSS Centre of Biological Signaling Studies, University of Freiburg, 79104 Freiburg Germany

§ These authors equally contributed to this work

Correspondence and requests for materials should be addressed to M.S.C (email: maria.carro@uniklinik-freiburg.de)

The authors declare no potential conflicts of interest.

ABSTRACT

Enhanced fatty acid synthesis is a hallmark of tumors, including glioblastoma. SREBF1/2 regulates the expression of enzymes involved in fatty acid and cholesterol synthesis. Yet, little is known about the precise mechanism regulating SREBP gene expression in glioblastoma. Here, we show that a novel interaction between the co-activator/co-repressor CTBP2 and the tumor suppressor ZBTB18 regulates the expression of SREBP genes. Our study points at CTBP2 as a co-activator of SREBP genes whose complex activity is impaired by ZBTB18. ZBTB18 binding to the SREBP gene promoters is associated with reduced LSD1 activity leading to increased di-methylation of lysine 9 (H3K9me2), and concomitant decrease of H3K4me3 with consequent repression of the SREBP genes. In line with our findings, lipidomics analysis shows a reduction of several phospholipid species upon ZBTB18 expression. Our results thus outline a new epigenetic mechanism enrolled by ZBTB18 and its cofactors to regulate fatty acid synthesis which could be targeted to treat glioblastoma patients.

STATEMENT OF SIGNIFICANCE

De novo lipogenesis is a hallmark of many cancers, including glioblastoma; therefore, revealing how fatty acid synthesis enzymes are regulated may open up new venues in therapy. Moreover, understanding how epigenetic control of key cancer genes occurs may contribute to shed light on common regulatory mechanisms shared by other tumor suppressors in different cancers.

INTRODUCTION

With a median survival of 15 months and a 5-year overall survival of 5.5%, glioblastoma (GBM) is the most aggressive and deadly type of brain tumor (1). Despite the aggressive treatments (surgery followed by chemo- and radio-therapy), the prognosis of GBM has not been improved over the past years, mostly because residual tumor cells are highly invasive and cannot be completely resected. In addition, a fraction of GBM cells acquire resistance to both chemotherapy and radiotherapy after being exposed to the treatments (2), thus, recurrent tumors usually become more aggressive.

Gene expression studies have highlighted the existence of a mesenchymal phenotype associated with the most aggressive glioblastoma features such as invasion and therapy resistance (3-6). Importantly, the acquisition of mesenchymal traits resembles the mesenchymal transition described in epithelial tumors and it is now considered a hallmark of aggressive tumors (7,8). Epigenetic changes in the cells are reversible covalent modifications which alter gene expression without changing the DNA sequence, and can be inherited by the cell progeny. An important layer of epigenetic modification is mediated by histone-modifying enzymes which add or remove acetyl or methyl groups in order to regulate chromatin accessibility to the transcriptional machinery. These enzymes usually interact with transcription factors, co-repressor or co-activators and represent an important therapeutic opportunity in cancer (9).

The C-terminal binding proteins (CTBP1/2) can function as co-repressors through association with DNA-binding transcription factors and recruitment of chromatin regulators such as histone deacetylases 1 and 2, (HDAC1/2), the histone demethylase KDM1A/LSD1, the histone methyltransferase PRC2 and the chromatin remodeling complexes NURD (10-13). Although usually described as a repressor, CTBP2 has been

also reported to act as a co-activator through the interaction with retinoic acid receptors (14) or through binding to the zinc finger protein RREB1 (11). CTBP2 has been also implicated in tumorigenesis and epithelial to mesenchymal transition (EMT) (15). In glioblastoma, CTBP2 has been shown to be highly expressed compared to lower grade tumors and to be associated with poorer prognosis (16).

Sterol regulatory element-binding proteins (SREBPs) are transcription factors which control the expression of enzymes involved in fatty acids and cholesterol biosynthesis (17,18). Three SREBP proteins have been identified in mammals; SREBP-1a and SREBP1-c, which result from alternative promoter usage of the SREBF1 gene (a.k.a. SREBP1), and SREBF2. SREBF1 isoforms regulate fatty acid synthesis while SREBF2 is implicated in cholesterol production (17). Fatty acid synthesis has been shown to play an important role in cancer including glioblastoma (19,20); excess of lipids and cholesterol in tumor cells are stored in lipid droplets (LD) which are now recognized as hallmarks of cancer aggressiveness (21-23). In glioblastoma, constitutive activation of EGFR (EGFRvIII mutant) leads to PI3K/AKT-dependent SREBF1 regulation with consequent increase in lipogenesis and cholesterol uptake which can be pharmacologically blocked by inhibiting the low-density lipoprotein receptor (LDLR), a SREBF1 target involved in cholesterol uptake (24). Moreover, blocking LD formation suppresses GBM lipogenesis and growth (25).

Previously, we have identified ZBTB18 as tumor suppressor in GBM which functions as a transcriptional repressor of mesenchymal genes and impairs tumor formation (26,27). Here, we have identified CTBP2 as a new ZBTB18-binding protein. We report that CTBP2 regulates the expression of fatty acid synthesis genes and that such activation is

opposed by ZBTB18 through the recruitment and inhibition of CTBP2 complex on SREBP genes promoters.

RESULTS

ZBTB18 interacts with CTBP2 through the VLDLS motif

With the goal to get a better insight into ZBTB18 transcriptional repressive mechanisms, we used Mass Spectrometry (MS) to identify ZBTB18 co-precipitated proteins in glioblastoma cells (SNB19), upon FLAG-ZBTB18 overexpression and subsequent anti-FLAG co-immunoprecipitation (Fig. 1A). Our data revealed that the corepressors CTBP1 and CTBP2 could be potential ZBTB18 interactors (Fig. 1B). CTBPs are co-repressors which are implicated in human cancer by promoting several pro-oncogenic activities including EMT, cell survival, migration and invasion (28-30). We validated the interactions by co-immunoprecipitation in multiple experiments using different antibodies directed to ZBTB18 or CTBP2 (Fig. 1C-D). CTBP1, on the other hand, appeared to bind to CTBP2 but not to ZBTB18 directly (data not shown). We also confirmed ZBTB18 interaction with CTBP2 in LN229 cells transduced with ZBTB18 (Supplementary Fig. S1A). Further MS analysis of endogenous ZBTB18 co-immunoprecipitation performed in a GBM-derived cell line (BTSC3082) detected CTBP1, but not CTBP2, in the co-precipitated fraction (Supplementary Fig. S1B-D), suggesting that ZBTB18 preferential interaction with CTBP2 or CTBP1 could be context-dependent. Interestingly, ZBTB18 protein sequence analysis revealed the presence of a putative CTBPs interaction motif (VLDLS) (Fig. 1E) (31). Substitution of the LDL amino acids into SAS amino acids by site directed mutagenesis completely abolished CTBP2 interaction with ZBTB18 (Fig. 1E-G), further supporting ZBTB18-CTBP2 interaction. We then looked at phenotypic

changes associated with ZBTB18 or ZBTB18-mut expressions in SNB19 cells. Consistent with our previous study (27), ZBTB18 affected cell proliferation, apoptosis and migration. ZBTB18 LDL mutant (ZBTB18-mut) also appeared to have a mild effect on apoptosis and proliferation while migration was not impaired (Supplementary Fig. S2), suggesting that the interaction with CTBP2 might be required for specific ZBTB18-driven tumor suppressive functions. Expression analysis of previously validated ZBTB18 mesenchymal targets, upon overexpression of the ZBTB18-mut showed that ZBTB18 interaction with CTBP2 is required for ZBTB18-mediated repression of a subset of targets (CD97, LGALS1 and S100A6, Fig. 1H), while repression of ID1, SERPINE1 and TNFAIP6 type of genes appears to be independent from CTBP2 binding. Interestingly, S100A6 and LGALS1 play an important role in glioma cells migration (32,33), consistent with our results (Fig. S2 E-F) and further reinforcing the idea that ZBTB18 interaction with CTBP2 may be crucial to regulate this property of mesenchymal GBMs. Overall these data identify CTBPs as new ZBTB18 interactors and suggest that ZBTB18 might employ both a CTBPs-dependent and a CTBPs-independent mechanism to repress target genes and mediate its tumor suppressor functions.

ZBTB18 and CTBP2 play an opposite role in gene regulation

To understand the role of CTBP2 and ZBTB18 interaction in gene regulation, we overexpressed FLAG-ZBTB18 and knocked down CTBP2, in SNB19 cells (Fig. 2A). Gene expression profiling followed by gene set enrichment analysis (GSEA) showed that both ZBTB18 overexpression and CTBP2 silencing similarly affected the expression of EMT gene signatures, suggesting an opposite role of CTBP2 and ZBTB18 in transcriptional regulation (Supplementary Fig. S3A). This is consistent with our reported

role of ZBTB18 as inhibitor of mesenchymal signatures in GBM and with previous studies indicating that CTBP2 promotes tumorigenesis and EMT (27,34).

Venn analysis of shCTBP2 and ZBTB18 regulated genes showed that about half of the genes regulated by shCTBP2 are also repressed by ZBTB18 overexpression (Fig. 2B, top panel). CTBP2 knockdown partially affected the portion of ZBTB18 regulated genes supporting the observation that ZBTB18 may regulate gene expression both in a CTBP2-dependent and independent manner (Fig. 2B, bottom panel). To identify new common pathways affected by ZBTB18 overexpression or CTBP2 knockdown, we looked at gene signatures which are up- or down-regulated by the two factors. GSEA revealed a strong loss of SREBP signaling genes expression both upon ZBTB18 overexpression and CTBP2 silencing (Supplementary Fig. S3B and Fig. 2C-D), according to a possible role of CTBP2 as co-activator, as previously shown (14), and of ZBTB18 as repressor. SREBP genes are involved in fatty acid uptake and synthesis. Notably, SREBPs function as master regulators of all the enzymes involved in the pathway (17). We focused on the SREBP signaling pathway given its importance in tumorigenesis and previous connection to EMT (35,36). Interestingly, GlioVis analysis (37) showed that SREBF1 is more highly expressed in the most aggressive GBM subtypes (mesenchymal and classical) compared to proneural GBMs, and correlates with patient survival (Supplementary Fig. S3C-D). Validation by qRT-PCR in SNB19 showed a strong reduction in the expression of all the genes tested upon ZBTB18 expression or CTBP2 silencing (Fig. 2E). Similarly, ZBTB18 expression led to downregulation of SREBP genes in LN229 cells and in primary GBM cells BTSC233 (Fig. S4A-B). In agreement with our microarray results, CTBP2 knockdown did not inhibit ZBTB18-mediated repression (Fig. 2D-E) but rather it further enhanced downregulation

of ZBTB18 target genes. Remarkably, treatment with the CTBPs inhibitor MTOB (38) also resulted in a strong downregulation of SREBP genes expression in SNB19 and BTSC 233 cells (Fig.2F and S4C). Consistent with our proposed role of CTBP2 as activator, we observed a strong positive correlation between CTBP2 expression in gliomas and the levels of all the SREBP genes tested (Gliovis platform, dataset CGGA (39), Fig.S5). When MTOB treatment was combined with ZBTB18 expression, no rescue of ZBTB18 repression was observed (Fig. 2G), further suggesting that CTBP2 and ZBTB18 independently regulate the same set of genes with opposite function (CTBP2 as an activator and ZBTB18 as a repressor) and excluding a role of CTBP2 as ZBTB18 corepressor. We then compared gene expression changes caused by ZBTB18 and ZBTB18-mut in SNB19 cells by qRT-PCR. Interestingly, the expression of some SREBP gene repressed by ZBTB18 (LDLR, GPAM, SQLE), was rescued when ZBTB18 lacked the CTBP2-interacting domain (Fig. 2H); on the other hand, the ZBTB18-induced repression of other genes (FASN, SREBF1, SREBF2, ACACA and SCD) was enforced even in the absence of CTBP2 interaction, indicating that ZBTB18 repression occurs through both CTBP2-dependent and CTBP2-independent mechanisms. Finally, we tested the effect of CTBP2 knockdown on tumor formation in mice xenograft. Following injection of shCtr-SNB19 cells all mice developed tumors while no tumor was detected in mice injected with SNB19-shCTBP2 cells. As a consequence SNB19-shCTBP2 survived longer ($p=0.039$) (Fig. 2I-K). These data further highlight the tumorigenic role of CTBP2 in contrast to ZBTB18 tumor suppressor function.

ZBTB18 and CTBP2 map to SREBP promoter regions

To further characterize the dynamics of CTBP2 and ZBTB18 on gene targets regulation, we mapped the genome wide distribution of CTBP2 and ZBTB18 by chromatin

immunoprecipitation coupled to deep sequencing (ChIPseq) in SNB19 cells. CTBP2 ChIP was performed with a CTBP2 antibody to precipitate the endogenous CTBP2 in absence or in presence of ZBTB18 (EV_CTBP2 and ZBTB18_CTBP2); while ectopic ZBTB18 was immunoprecipitated with FLAG antibody (EV_FLAG and ZBTB18_FLAG). After subtracting FLAG unspecific peaks detected in SNB19-EV_FLAG, we performed Venn analysis of all the annotated peaks (Fig. 3A). We found 5361 peaks shared by all conditions suggesting that CTBP2 and ZBTB18 bind to the same gene regions (Fig. 3B). Remarkably, peaks which are in common with all the conditions (All) and between ZBTB18 and CTBP2 in the presence of ZBTB18 (Not_EV-CTBP2) were strongly enriched at promoter regions in close proximity to the transcription start (Fig. 3C-D). Analysis of published ChIP-seq datasets using ReMap (40) showed a good overlap between shared CTBP2 and ZBTB18 promoter peaks, with peaks for known CTBP2 interactors such as NCOR1, ZNF217 and LSD1/KDM1A (Supplementary Fig. S6A). When focusing on SREBP gene promoters, we observed a strong consensus between peaks identified in ZBTB18 (FLAG) and CTBP2 ChIPs (Fig. 3E and Supplementary Table S1), again suggesting that CTBP2 and ZBTB18 play a direct role in SREBP genes transcription. Furthermore, SREBP genes peaks common to ZBTB18 and CTBP2 ChIPs, matched with genes regulated by CTBP2 silencing and ZBTB18 overexpression in our gene expression analysis (INSIG1, SREBF1, FASN, ACACA, LDLR, DBI, SCAP, SQLE and SCD; Fig. 2D-E, Fig. 2G and Fig. 3F and Supplementary Table S1). These results further reinforce the notion that CTBP2 and ZBTB18 bind to the same gene promoters; in addition, this constitutes the first genome wide mapping of CTBP2 and ZBTB18 in glioblastoma cells.

We further confirmed the binding of ZBTB18 to the promoter of a set of SREBP genes by qChIP analysis (Fig. 3G). Upon overexpression in SNB19 cells, ZBTB18 is recruited to the promoter region of all analyzed genes but not of CyA151, which is a preferential target of CTBP2 alone (Fig. 2D). CTBP2 is present at the promoter of SREBP genes in the absence of ZBTB18 (Fig. 3H) where according to our microarray analysis and qPCR results (Fig. 2D-E), it is responsible for their transcriptional activation. Interestingly, we observed a consistent increase of CTBP2 levels at the promoter of SREBP genes in the presence of ZBTB18 (Fig. 3H) suggesting that the interaction between ZBTB18 and CTBP2 adds complexity to the regulatory dynamics of the latter.

ZBTB18 facilitates CTBP2 binding to ZNF217, LSD1 and NCOR1

To better understand whether the presence of ZBTB18 affects CTBP2 interaction with other proteins, we performed SILAC-based MS in SNB19 cells transduced with either control vector (low-weight medium, L) or ZBTB18 (high-weight medium, H) followed by CTBP2 co-immunoprecipitation (Fig. 4A). Interestingly, ZNF217, RCOR1, LSD1/KDM1A and HDAC1/2, which are well characterized CTBP2 and CTBP1 interactors, more efficiently co-precipitated with CTBP2 when ZBTB18 was expressed (H/L=1.83, 1.73,1.6 and 1.48 respectively) (Fig. 4B). CTBP2 co-immunoprecipitation in SNB19 cells followed by western-blot analysis confirmed the increased binding of ZNF217 and LSD1 to CTBP2 upon ZBTB18 expression (Fig. 4C). These pieces of evidence suggest that CTBP2 complex dynamics and functions could change upon ZBTB18 overexpression. We then performed ChIP analysis of LSD1 and ZNF217 in SNB19 cells transduced with either control vector (EV) or ZBTB18 (Fig. 4D-E). Interestingly, both LSD1 and ZNF217 appeared to be more enriched at SREBP gene promoters when ZBTB18 was expressed in agreement with our previous results of an enhanced binding of these factors to

CTBP2 in the presence of ZBTB18. H3K9me2 is a well-established target of LSD1 demethylase activity and a marker of heterochromatin widely linked with transcriptional repression (41). Therefore to verify whether LSD1 demethylase function is critical for ZBTB18-induced gene repression, we measured H3K9me2 enrichment at the promoter of the SREBP genes. H3K9me2 levels were increased for all the tested genes upon ZBTB18 overexpression (Fig. 4F). A possible explanation is that the recruitment of CTBP2 complex by ZBTB18 to its target sites inhibits LSD1 demethylase activity and might be employed by ZBTB18 to counteract CTBP2-mediated activation. In line with this and with the role of ZBTB18 as a repressor of SREBP genes expression, we observed that the levels of H3K4me3, a well-known marker of transcriptional activation, were decreased at the promoters of all the analyzed genes (Fig. 4G). To verify whether ZBTB18 binding to CTBP2 is required for the recruitment/stabilization of the CTBP2 complex, ChIP experiments on selected SREBF1 genes were repeated in presence of ZBTB18-mut. Interestingly, recruitment of CTBP2, LSD1 and ZNF217 at the SREBP promoters was impaired upon ZBTB18-mut expression compared to ZBTB18-transduced cells (Fig. 4H and Supplementary Fig. S6B-D). Consistently, H3K9me2 enrichment reverted to the EV condition (Fig. 4I) suggesting that inhibition of LSD1 activity by ZBTB18 activity requires CTBP2 binding. Finally, we measured LSD1 activity in SNB19 nuclear extracts upon ZBTB18 and ZBTB18-mut expression or treatment with the LSD1 inhibitor RN-1. Remarkably, LSD1 activity was strongly impaired as a consequence of ZBTB18 expression but not by ZBTB18-mut which seemed to further activate it (Fig. 4J). Taken together, these results show that ZBTB18 represses transcription of SREBP genes by inhibiting CTBP2 complex activity and by affecting the level of histone modifications at the promoter region of target genes. These findings are

also in agreement with and further strengthen our microarray analysis showing silencing of common genes upon ZBTB18 overexpression and CTBP2 knockdown.

ZBTB18 affects lipid synthesis

Then, we investigated whether ZBTB18 overexpression caused phenotypic changes associated with decreased fatty acid synthesis, as a consequence of deregulated SREBP signaling gene expression. SNB19 cells were transduced with ZBTB18 or ZBTB18-mut and lipidome profiling was performed by a targeted LC-MS method, which had been verified by a Waters Synapt G2Si (Fig. 5A). Hierarchical clustering of the significantly altered lipids highlighted that ZBTB18-expressing cells segregated together with each other and separately from the other samples (EV and ZBTB18-mut) regardless of the growing conditions (normal medium or lipid-depleted medium) (Supplementary Fig. S7A and 5B). Within this cluster, the significantly regulated lipid species were largely underrepresented in the ZBTB18-expressing cells compared to the EV control cells; notably, the trend was more extreme in conditions of lipid starvation. A second cluster included EV control cells and ZBTB18-mut-expressing cells grown in normal medium. A third cluster comprised EV control cells and ZBTB18-mut-expressing cells grown under lipid starvation conditions. While in the presence of lipids in the culture medium both EV- and ZBTB18-mut-expressing cells where characterized by a very similar pattern of lipid abundance, when grown in lipid-depleted medium, the two cell types differentiated from each other with ZBTB18-mut-expressing cells showing the highest variation of lipid abundance compared to their counterparts grown under normal conditions.

In order to estimate the relative expression of the lipid species, the samples for each growing condition were normalized by the average lipid concentration measured in the

respective EV control cells (Supplementary Fig. S7B and 5C). As a result of this additional calculation, the number of lipid species differentially represented which reached the significance threshold, decreased. Two main clusters emerged from this analysis: the first one included ZBTB18-expressing cells grown under both conditions and lipid-starved ZBTB18-mut-expressing cells, the second group contained EV controls grown under both conditions and ZBTB18-mut-expressing cells grown in normal medium (Supplementary Fig. S7B). With the exception of myristic acid (14:0), all other significantly regulated lipid species were underrepresented in the ZBTB18-expressing samples, in condition of lipid starvation especially, further confirming the inhibitory effect of ZBTB18 on lipids synthesis. Interestingly, the concentration of these lipid species in ZBTB18-mut-expressing cells was similar to that of the EV controls under normal growing conditions, but dropped to the level of the ZBTB18-expressing ones, when the cells were kept in lipid-depleted medium (Fig. 5C).

ZBTB18 overexpression reduces lipid storage

Then, we analyzed lipid droplets content in tumor cells upon ZBTB18 or ZBTB18-mut overexpression. ZBTB18 overexpression diminished the amount of lipid droplets within the cells; however, the reduction was only slight and not significant under normal conditions. The difference became more evident and significant after the cells were lipid starved for 48 hours: under these conditions, the lipid droplet content of EV control cells remained unaltered, while in ZBTB18-expressing cells it was significantly decreased (Fig. 6A-B). Interestingly, the cells expressing ZBTB18-mut showed behavior similar to that of the EV controls, suggesting CTBP2-binding capability is required for ZBTB18 to exert its role in controlling lipid accumulation. Moreover, when lipid-starved, ZBTB18-expressing cells were incubated with lipid-containing medium again, they showed a

significant increment of lipid droplets albeit not fully recovering to the level of the EV controls (Fig. 6A-B). This observation suggests that the loss of lipid droplets in cells expressing ZBTB18 is mostly due to the blockade of the lipid biosynthesis on which tumor cells especially rely when there are no lipid sources available in the environment. To verify this hypothesis, we assessed the capability of the cells to intake fluorescently labelled palmitic acid (Bodipy-C16). In agreement with previous data, no significant difference was observed in the lipid uptake regardless of the overexpression of ZBTB18 or ZBTB18-mut (Fig. 6C).

Taken together, these data suggest that ZBTB18 plays an important role in controlling lipid metabolism of GBM cells. In addition, the results collected from ZBTB18-mut-expressing cells suggest that CTBP2 binding to ZBTB18 is, to some extent, required in order to affect the lipid metabolism of the tumor cells, however the exact roles played by these two interactors in the different aspects of lipid biosynthesis and storage remain to be fully clarified.

ZBTB18 overexpression alters cell metabolism

Since fatty acids can be used by the cell to fuel mitochondrial respiration, we investigated whether ZBTB18 regulation of the lipid biosynthesis could affect the metabolism of GBM cells. Oxygen consumption rate (OCR) and extracellular acidification rate (ECAR) were measured to determine the ATP production rate in control or ZBTB18 expressing SNB19 cells cultured in normal conditions or in lipid starvation. ZBTB18 expressing cells showed a lower ATP production rate compared to control cells; moreover, the depletion of external supply of lipids diminished the overall ATP production with the starkest reduction observed in the ZBTB18 expressing cells (Fig. 7A, S8A). In depth analysis of the ATP production rate showed that whereas the glycolytic

contribution remains constant between samples in normal conditions and in lipid starvation, the contribution of mitochondrial respiration was significantly decreased, especially in ZBTB18 expressing cells (Fig. 7A, S8B-C). As a result, when exposed to limited external supply of lipids, ZBTB18 expressing cells showed a more prominent shift from an energetic phenotype to a glycolytic one compared to control cells (Fig. 7B). Overall, our data suggest that the blockade to lipid biosynthesis elicited by ZBTB18 overexpression may prevent the tumor cells from fueling the aerobic respiration with fatty acids, when there is no external source available.

DISCUSSION

Here, we have identified a new role of ZBTB18 and CTBP2 in the regulation of fatty acids synthesis which is considered a hallmark of cancer, including glioblastoma. We show that the tumor suppressor ZBTB18 interacts with the cofactor CTBP2 and represses the expression of SREBP genes, involved in *de novo* lipogenesis. In the absence of ZBTB18, CTBP2 activates the expression of SREBP genes; while when it is present, ZBTB18 blocks their expression by inhibiting CTBP2-associated complex activity. Consistent with such a new function, ZBTB18 expression is accompanied by the reduction of several phospholipid species which rely on fatty acids availability to be assembled, and by altered metabolic activity and decreased lipid droplet content inside the cells (Fig.7E).

We show that ZBTB18 binding to CTBP2 is mediated by the VLDLS domain, a region previously shown to be required for interactions with CTBP1/2 (42). The interaction between ZBTB18 and CTBP2 initially prompted us to consider CTBP2 as a putative ZBTB18 corepressor. However, genome-wide gene expression analysis indicated that

ZBTB18 and CTBP2 play an opposite role in the transcriptional regulation of a common set of genes. Among them, EMT and SREBP genes are highly represented and appeared to be activated by CTBP2 and repressed by ZBTB18. Interestingly, many studies focusing on cell differentiation have shown that CTBP2 can prime its position in actively transcribed genes and that CTBP2 binding to different transcription factors can cause the switch to a repressive state (10,13). Several studies have shown that CTBP2 can be part of activator complexes; for example, CTBP2 and its associated proteins, LSD1 and NCOR1, have been implicated in transcriptional activation by the basic helix-loop-helix transcription factor NeuroD1, in gastrointestinal endocrine cells (11). This is consistent with the dual role of LSD1 in transcriptional activation and repression (43,44). In addition, CTBP2 has been reported to act as a co-activator of retinoic acid receptor (RAR)(14). Of note, a role of RAR in the regulation of FASN and ABCA1, two SREBP genes, has been previously described (45,46). Therefore, it is possible that RAR or other TFs, including SREBF1, could mediate SREBP genes activation by recruiting the CTBP2-LSD1 complex and that this activity could be blocked by ZBTB18.

Our further analysis suggests that ZBTB18 could interfere with CTBP2 transcriptional activation of SREBP genes by inhibiting the enzymatic activity of its associated complex, including LSD1-mediated demethylation of H3K9me2. Interestingly, LSD1 has been shown to regulate the expression of the fatty acids synthase enzyme FASN and consequently, triglyceride levels in hepatocytes (47). Furthermore, the study shows that LSD1 histone-demethylase activity is required for the regulation of lipogenic gene expression; this is consistent with our data showing that ZBTB18 expression leads to increased H3K9me2, as consequence of LSD1 inhibition. H3K9me2 is a histone modification specifically associated with transcriptional repression via the induction of

heterochromatin formation (41). Interestingly, both positive and negative changes of H3K9me2 have been implicated in the development and progression of various types of cancer due to its influence on cell differentiation, apoptosis, and treatment response (48-50). Thus, the role of H3K9me2 in promoting or restringing cancer might depend on the genomic context as well as on the activity of specific histone methylation and demethylation enzymes.

Recently, CTBP2 has been linked to the inhibition of cholesterol synthesis in breast cancer cells through direct repression of SREBF2 expression (51). In addition, the authors suggest that fatty acid synthesis could be affected since SREBF1 is also repressed. Although apparently in contrast with our proposed role of CTBP2 as activator of SREBP genes; it is possible that such a mechanism may be specific for breast cancer cells and depend on CTBP2 interaction with ZEB1. According to this possibility, ZEB1 was never detected in our CTBP2 co-immunoprecipitation analysis in glioblastoma cells.

De novo production of fatty acid, also known as “lipogenic phenotype” is recognized as an important hallmark of tumor cells, including glioblastoma (52). Our lipidome analysis shows that expression of ZBTB18 in GBM cells affects the synthesis of phospholipids, in particular those containing unsaturated fatty acids. An elevated phospholipid production rate is a trait of rapidly dividing cells, such as tumor cells, because they are required to form the cellular membranes of the new cells. The reduced amount of several phospholipid species upon ZBTB18 ectopic expression might be linked to the previously observed decreased proliferation rate of these cells (27).

It has been previously reported that malignant glioma tissues contain high levels of polyunsaturated fatty acids (53,54). Since the SREBF1 target SCD converts newly synthesized saturated fatty acids to unsaturated fatty acids (55,56) it is possible that

ZBTB18-mediated SCD repression accounts for the observed reduction of unsaturated and polyunsaturated fatty acids.

The expression of ZBTB18 in GBM cells also led to a reduced amount of lipid droplets, the intracellular organelles in which neutral lipids are stored. The abundance of lipid droplets within the cell depends on several factors including *de novo* lipid synthesis, uptake of lipids from the environment, and mobilization rate, according to the lipid demand for cellular functions (57). In our experimental model, the effect of ZBTB18 on the lipid droplets became evident when the cells lacked an external source of lipid, and additionally, ZBTB18 overexpression seemed not able to hinder the lipid uptake from the environment. This suggests that ZBTB18 specifically affects the lipid biosynthesis but not the ability of GBM cells to gather lipids from external sources. In fact, while most of the cells rely on external sources of fatty acids to satisfy their needs, cancer cells have been shown to be able to synthesize their own lipids and recent studies have provided evidence of a relevant role of fatty acid oxidation on GBM tumor growth (58). When ZBTB18 expression is restored in GBM cells, the process of lipid biosynthesis appears to be broken, theoretically forcing the cells to be more dependent on extracellular fatty acid supply. This observation is supported by the dramatic reduction of ATP produced by mitochondrial respiration when ZBTB18 expressing cells are deprived of an external source of lipids. In addition, the increased saturation of the phospholipid chains caused by SCD downregulation has been shown to disrupt mitochondrial functions (59); this might also contribute to reducing ATP production derived from oxidative phosphorylation upon ZBTB18 ectopic expression. These data hint that potential therapies targeting ZBTB18-CTBP2 complex could be more effective if supported by adjuvant treatments to prevent extracellular lipid uptake and possibly, to block also the glycolytic component of

ATP production which does not seem to be affected by either ZBTB18 expression or lipid depletion.

In conclusion, we unravel a new epigenetic mechanism of transcriptional regulation employed by the tumor suppressor ZBTB18 to repress SREBP genes and *de novo* lipogenesis in glioblastoma cells. Epigenetic changes have emerged to be a critical step for tumorigenesis and metastasis but the key epigenomic events in cancer cell transformation still remain poorly understood. Our findings contribute to better understand how epigenetic regulation of key cancer genes occurs and may constitute a common mechanism shared by other tumor suppressors. Given the role of ZBTB18 as a negative regulator of the mesenchymal transformation in GBM, our results have important implications in cancer therapy as they might help to find more effective strategies to diagnose and treat glioblastoma. Furthermore, given the recognized oncogenic role of CTBP2, LSD1 and ZNF217 in other cancers, their implication in *de novo* lipogenesis could have a broader impact in cancer research.

ACKNOWLEDGMENT

We thank Mahmoud Abdelkarim and Jonathan Goldner for technical assistance. We thank Veronica Dumit and Lisa Winner (University of Freiburg, ZBSA) for MS analysis, Katrin Seidel for mice brain histology and Olaf Gross and Oliver Gorka for use of the Seahorse XF and for advice. We are grateful to Marc Timmers for advice and discussion. The results shown here are in part based upon data generated by the TCGA Research Network: https://www.cancer.gov/tcga. This work is supported by the German's Cancer Aid grant (Deutsche Krebshilfe, 70113120) to MSC.

MATERIALS and METHODS

Cell culture

SNB19, LN229 and HEK293T cells were cultured in DMEM supplemented with Glutamax (Life Technologies), 10% fetal bovine serum and 1% Penicillin/Streptomycin at 37°C. For lipid starvation, SNB19 cells were grown in DMEM supplemented with 10% lipids depleted FBS (Biowest). Primary glioblastoma cells BTSC233 were generated in our laboratory in accordance with an Institutional Review Board-approved protocol (27). BTSC3082 were generated at the University of Uppsala (60) and kindly provided by Dr. Nelander. BTSC233 and BTSC3082 were grown in Neurobasal medium (Life Technologies) containing B27 supplement (Life Technologies), FGF (20 ng/ml, R&D Systems), EGF (20 ng/ml, R&D Systems), (LIF 20 ng/ml, Genaxxon Biosciences), Heparin (2 μg/ml, Sigma), and glutamax (Invitrogen). BTSC3082 were grown adherent on dishes previously coated with laminin (Life Technologies). All cells were mycoplasma-free. SNB19 LN229 and HEK293T cells have been authenticated on 3/2/2017 (SNB19 and LN229) and on 11/26/19 (SNB19 and HEK293T) by PCR-single-locus-technology (Eurofins Medigenomix). For CTBP1/2 inhibition, SNB19 and BTSC 233 cells were treated with 10 mM 4-methylthio-2-oxobutyric acid (MTOB, Sigma) for 24h.

Vectors and Viral Infection

To produce FLAG-ZBTB18-HisZBTB18, ZBTB18 was PCR amplified from the previously described pCHWMS-eGFP-ZBTB18 lentiviral vector (27) using primers containing a BstXI and PmeI restriction sites. Upon restriction digestion the ZBTB18 fragment was cloned into BstXI and PmeI sites by removing the LUC region of the PCHMWS-eGFP-IRES vector. Primers are listed in the reagent table. ZBTB18 LDL-mut was obtained by

site-directed mutagenesis using pCHWMS-eGFP-FLAG-ZBTB18-His as template and the QuikChange II XL Site-Directed Mutagenesis kit (Agilent), according to the manufacturer's instructions. All constructs were sequence validated. Primers are listed in Supplementary Table S2.

Lentiviral stocks and cell infection were performed as previously described (27). Ectopic protein expression was determined by immunoblotting with an anti-Flag M2 antibody (Sigma). For CTBP2 knockdown, CTBP2 short hairpin cloned in the pLKO lentiviral vector was used (Sigma, #TRCN0000013745). Lentiviral particles were generated in HEK293T cells as previously described (27). Selection of infected cells was conducted with 2 μg/ml of Puromycin (Sigma).

RNA extraction and quantitative real time-PCR

Total RNA was extracted from cell culture using miRNeasy Mini Kit (Qiagen) according to the manufacturer's instructions. First strand cDNA synthesis was generated using the Superscript III First-Strand Synthesis System for RT-PCR (Life Technologies) following the manufacture's protocol. Quantitative RT-PCR was performed using Kapa SYBR Fast (Sigma). SREBP genes primer sequences are listed in Table S2. Primers for SERPINE1, TNFAIP6, CD97, LGALS1, S100A6 and ID1 were previously described (27).

Gene expression analysis

For gene expression analysis, 1.5 µg of total RNA was processed and analyzed at the Deutsches Krebsforschungszentrum (DKFZ) in Heidelberg (Germany). Hybridization was carried out on Illumina HumanHT-12v4 expression BeadChip. Microarray data were further analyzed by gene set enrichment analysis (GSEA) (http://www.broadinstitute.org/gsea/index.jsp). Microarray gene accession number: GSE138890. Differentially regulated genes were identified using the limma R package

(61). Genes with adjusted pvalue < 0.05 and absolute fold-change > 0.5 were considered as significantly regulated. A gene-sets enrichment analysis was performed using Fisher's exact test on the Consensus Path DB (62), comparing these selected genes against the whole set of quantified genes. Significance threshold was set to adjusted pvalue < 0.05. gene correlation, SREBF1 gene expression and patient survival analysis was performed using the GlioVis platform (37) and data from The Cancer Genome Atlas (TCGA) (https://www.cancer.gov/tcga) and Chinese Glioma Genome Atlas (CGGA) project (39).

Immunoblotting

Total protein extracts were prepared in RIPA buffer supplemented with Halt™ protease and phosphatase inhibitor cocktail (Thermo Scientific), and PMSF (Sigma). Protein lysates were quantified using the Bradford method. Proteins were resolved in SDS-PAGE, transferred to a Nitrocellulose Blotting Membrane (Amersham) and exposed to the following primary antibodies: mouse anti-FLAG (Sigma #F1804), rabbit anti FLAG (Cell Signaling #2368S), rabbit anti-ZBTB18 (AbCam #ab118471), mouse anti-CTBP2 (BD Biosciences #612044), rabbit anti-LSD1 (Millipore #17-10531), rabbit anti-ZNF217 (Thermo Fisher scientific #720352) and mouse anti alpha tubulin (Abcam #ab7291). Membranes were treated with corresponding horseradish peroxidase-conjugated secondary antibodies (Santa Cruz, #sc-2031and #sc-2313) and developed using the Bio-Rad clear ECL substrate (Bio-Rad).

Intracranial injection and histology

SNB19 cells transduced with either shCtr or shCTBP2 (1x105) were injected in the striatum of NOD/SCID female mice as previously described (26) and in accordance with

the directive 86/609/EEC of the European Parliament, following approval by regional authorities. Histology was performed as previously described (63).

Co-immunoprecipitation and mass spectrometry and SILAC

For co-immunoprecipitation (co-IP) SNB19 or LN229 cells were lysed in co-IP buffer (150 mM NaCl, 50 mM TrisHCl pH 7.5, 10% glycerol, 0.2% Igepal, 1mM EDTA) supplemented with Halt™ protease and phosphatase inhibitor cocktail (1mM, Thermo Scientific), and PMSF (1mM, Sigma). The cell pellets were resuspended in 1 ml each of the cell lysis mix, vortexed for 30 seconds and kept on ice for 30 minutes. After centrifugation at 13,200 rpm for 20 minutes at 4°C a pre-clearing step was performed by adding 25 µl of Protein A/G PLUS-Agarose beads (Santa Cruz) and incubating the samples for 1 hour at 4°C in rotation. The recovered supernatant was then incubated overnight with the specific antibodies: rabbit anti-CTBP2 (Cell Signaling #13256S), mouse anti-FLAG (Sigma # F1804), rabbit anti-ZBTB18 (AbCam #ab118471). Normal mouse IgG or normal rabbit IgG were include as controls (Santa Cruz, #sc-2025 and # sc-2027). 20 µl of lysate (input) were removed and mixed with equal volume of 2X laemmli buffer for western blot analysis. At the end of the overnight incubation 20 µl of equilibrated protein A/G beads were added to each lysates and incubated for 2 hours at 4°C. The beads were then washed for 4 times with 1 ml of co-IP buffer before eluting the co-precipitated proteins with 20 µl of 2X laemmli buffer. The mixture was vortexed for 30 seconds and heated at 95°C for 5 minutes to detach proteins from the beads. Samples were stored at -20°C or directly analyzed by western blot. For mass spectrometry (MS) analysis, samples were prepared as described in (64) and then measured on a LTQ Orbitrap XL (Thermo Scientific) instrument at the Core Facility Proteomics of the Center for Biological System Analysis (ZBSA) at the University of Freiburg (Freiburg, Germany).

Data acquisition and analysis was performed using Xcalibur (Thermo Scientific, Germany) and MaxQuant 1.4.1.2 softwares. For ZBTB18 co-IP in BTSC3082, cells were lysed as described above and lysates were incubated overnight with rabbit anti-ZBTB18 (Proteintech #12714-1-AP). The eluted co-precipitated proteins were separated by gel electrophoresis and gel fragments were processed at the Core Facility Proteomics at the University of Freiburg as described above. CTBP1 interaction was validated by western blot with mouse anti-CTBP1 (BD Biosciences #612042).

To run SILAC, SNB19 cells were SILAC labelled using Arg0/Lys0 (low, L) and Arg10/Lys8 (high, H) (Silantes). Afterwards cells were transduced with pCHMWS-EV (L) or pCHMWS-FLAG-ZBTB18 (H) lentiviral particles prepared as described above. Transduced SNB19 were mixed and lysed in co-immunoprecipitation buffer as described above. Total protein extracts were incubated with rabbit anti-CTBP2 (cell Signaling #13256S) and the precipitated fraction subjected to MS to identify interacting proteins and calculate H/L ratios. Measurement and analysis were performed at the Core Facility Proteomics of the Center for Biological System Analysis (ZBSA) at the University of Freiburg (Freiburg, Germany) as described above. The protein interactions from this publication have been submitted to the IMEx (www.imexconsortium.org) consortium through IntAct (65) and assigned the identification number IM-27496.

Migration, proliferation and apoptosis assay

In a wound healing assay, SNB19 transduced cells were plated in 6-well plates and grown to 95% confluence. A scratch of approximately 1 mm was made with a p1000 pipette tip and images were taken at 0, 5, 24 and 30 hours using a microscope (Axiovert, Zeiss). Cell migration was calculated using the following formula: (Pre-Migration Area – Migration Area)/Pre-Migration Area).

Cell proliferation was assessed using a commercially available kit for EdU detection (EdU Cell proliferation assay, Baseclick). SNB19 cells were transduced and plated at a density of $2.5x10^4$ per well in a 4 well chamber slide (Lab-Tek). After 24 hours of seeding, cells were incubated with EdU solution overnight following the manufacturer's instructions. Upon EdU detection, images were acquired using a fluorescent microscope (Axiovert, Zeiss) and positive EdU cells were counted.

For apoptosis assay, transduced SNB19 cells were seeded in a 96 well (dark plate) at a density of $1x10^3$ per well. The following day activity of caspases 3 and 7 was measured using the Caspase-Glo® 3/7 Assay (Promega), according to the manufacturer's instruction.

LSD1 activation assay

For LSD1 activity assay, SNB19 cells were transduced with EV, ZBTB18 or ZBTB18-mut as described above or treated with 5 μM RN-1 inhibitor (Calbiochem) for 96h. Nuclear lysates were prepared with EpiQuik™ Nuclear Extraction Kit (Epigenetk). Measurement of LSD1 activity was performed with Epigenase LSD1 Demethylase Activity/Inhibition Assay Kit (Epigentek) according to the manufacturer's instructions. LSD1 activity was quantified by Infinite 200 PRO Spectrophotometer (Tecan) at 450 nm and 655 nm, following the manufacturer's instructions.

Quantitative ChIP and ChIP-seq

Quantitative ChIP was performed as follows: SNB19 cells were seeded at $1x10^6$ cells confluency and transduced either with the control or ZBTB18 expressing lentiviral vectors as described before. After 72 hours cells were washed in PBS and incubated in the presence of ChIP Crosslink Gold solution (Diagenode) for 30 minutes at room temperature to enhance protein-protein interactions, fixed by addition of 1%

formaldehyde for 20 minutes at room temperature and quenched by addition of PBS for 5 minutes. The cells were resuspended in 2 ml L1 buffer (50 mM Tris pH 8.0; 2 mM EDTA pH 8.0; 0,1% NP40; 10% glycerol; protease inhibitors) per 10^7 cells, and lysed on ice for 5-10 minutes. The nuclei were collected by centrifugation at 800g for 5 minutes at 4°C and lysed in 1 ml of L2 buffer (0,2% SDS; 10 mM EDTA; 50 mM Tris pH 8; protease inhibitors). The suspension was sonicated in a cooled Bioruptor Pico (Diagenode), and cleared by centrifugation for 10 minutes at 13000 rpm. The chromatin (DNA) concentration was quantified using NanoDrop (Thermo Scientific) and the sonication efficiency monitored on an agarose gel. Protein A sepharose (PAS) beads (GE Healthcare) were blocked with sonicated salmon sperm DNA (200 mg/ml beads) and BSA (250 mg/ml beads) in dilution buffer (0.5% NP40; 200 mM NaCl; 50 mM Tris pH 8.0; protease inhibitors) for 2 hours at room temperature. The chromatin was diluted 10x in the dilution buffer and pre-cleared with blocked PAS for 1 hour at 4°C. 5 ug of pre-cleared chromatin was incubated with 5 ug of antibody O/N at 4°C, then with 40 ul of blocked PAS further 2 hours at 4°C. The following antibodies were used: rabbit anti-CTBP2 (Active Motif #61262), mouse anti-FLAG (Sigma #F1804), rabbit anti-LSD1 (Merck Millipore #17-10531), rabbit anti-ZNF217 (Thermo Fisher Scientific #720352), rabbit anti-H3K4me3 (Diagenode #C15410003) and rabbit anti-H3K9me2 (Cell Signaling #9753). Control mock immunoprecipitation was performed with blocked PAS. The beads were washed 4x with WB-250 (0.02% SDS; 0.5% NP40; 2 mM EDTA; 250 mM NaCl; 20 mM Tris pH 8.0). The immuno-complexes were eluted by two 15 minutes incubations at 30°C with 100 µl elution buffer (1%SDS, 100mM $NaHCO_3$), and de-crosslinked overnight at 65°C in the presence of 10U RNase (Roche). The immunoprecipitated DNA was then purified with the QIAquick PCR purification kit (Qiagen) according to

manufacturer's protocol and analyzed by quantitative real-time PCR. Primers are listed in Table S2. For ChIP-seq, SNB19 cells were transduced and incubated with ChIP Crosslink Gold solution (Diagenode) as described before, and processed using the iDeal ChIP-seq kit for Transcription Factors (Diagenode), according to the manufacturer's instruction. The following antibodies were used: rabbit anti-CTBP2 (Active Motif #61261) and mouse anti-FLAG (Sigma #F1804). Libraries preparation and ChIP-seq were performed by the Diagenode Company (https://www.diagenode.com). ChIPseq gene accession number: GSE140002Downstream analyses were performed with R (3.6.0). With the ChIPpeakAnno R package (66) we performed the Venn analysis where a single base overlap threshold was used to identify the common peaks between the 3 conditions (i.e. EV CTBP2, ZBTB18 CTBP2 and ZBTB18 FLAG). Peaks were divided according to the Venn subgroups and annotated with the nearest gene using ChIPseeker [(67)] and TxDb.Hsapiens UCSC.hg19.knownGene R packages. Enrichment analysis of gene-regions was done via a Fisher's exact test using 100 000 regions of 200bp, randomly selected on the human genome, as background. ReMap (40) was used to look at overlap with other TFs and cofactors peaks from published data in other cell lines.

Lipidomics Analysis

For lipid profiling, cells were washed, quenched and lysed as previously described (68) and lipids were extracted as described by (69). Internal standard containing organic phase was evaporated to dryness and reconstituted in isopropanol:acetonitrile:water 2:1:1 and subjected to targeted LC-MS lipid profiling. A BEH C18 2.1 mm x 100 mm, 1.8 µm column (Waters Corporation) was used with the following chromatographic program: 40 % solvent B (10 mM NH_4CHO_2, 0.1% formic acid, isopropanol:acetonitrile

9:1) was hold for 2 minutes, to 98% B within 10 minutes, hold for 2 minutes, to 40% B within 0.5 minutes and hold for 5.5 minutes. Solvent A was 10 mM NH_4CHO_2, 0.1% formic acid, acetonitrile:water 3:2. The flow rate was set to 300 µl/minute and the column temperature was 55°C. The method was further verified by analyzing lipid standards with the same chromatography coupled to a high resolution mass spectrometer (Synapt G2Si, Waters Corporation). Samples were kept at 12°C and injected in randomized order with pooled quality control samples injected at regular intervals. Lipids were monitored by MRM and SIM scan modes using an Agilent 6460 triple quadrupole. Raw data were analyzed by Agilent Quantitative Analysis software. Samples were normalized to internal standard, QC-filtered and range-scaled for principal component analysis and heat map generation. Significance was determined by ANOVA including FDR multiple testing correction (q-value cut off: 0.05). Statistical analyses and visualization were carried out by MetaboAnalyst 4.0 (70).

Immunostaining and lipid staining

After SNB19 cells had been infected as described above, they were maintained in 4-well chamber slides either with 10% FBS DMEM or 10% lipid-depleted FBS DMEM for 48 hours. The cells that underwent lipid starvation were then kept for additional 2 hours either in 10% lipid-depleted FBS DMEM or in 10% FBS DMEM, to allow them to intake the lipids from the environment and recover from the deprivation. Control cells grown in 10% FBS DMEM were also kept for additional 2 hours without changing the medium. The cells were then fixed with 4% paraformaldehyde in PBS and processed for the staining. ZBTB18 was labelled with anti-ZBTB18 rabbit polyclonal primary antibody (Proteintech #12714-1-AP) and anti-Rabbit IgG (H+L) Alexa Fluor 647 (goat, Thermo Fisher Scientific) secondary antibody. Lipid droplets were stained with 0.5 µg/ml Bodipy

TMR-X SE (Thermo Fisher Scientific) in 150 mM NaCl for 10 minutes at room temperature. Nuclei were counterstained with 4′,6-diamidino-2-phenylindole (DAPI, Sigma-Aldrich). Pictures were acquired using a FSL confocal microscope (Olympus).

Lipid uptake

SNB19 cells were seeded in 4-well chamber slides and infected as described above. The cells were then incubated with 50 nM Bodipy-C16 (Thermo Fisher Scientific) in PBS for 15 minutes at room temperature. Subsequently, the samples were fixed with 4% paraformaldehyde in PBS, counterstained with DAPI and imaged using a FSL confocal microscope (Olympus).

Metabolic assays

Oxygen consumption rate (OCR) and extracellular acidification rate (ECAR) were measured using the Seahorse XFe 96 Extraflux Analyzer (Agilent Technologies, Lexington, MA) to evaluate the metabolic profile of GBM cells. The assays were carried on according to manufacturer's instructions. Briefly, the cells (SNB19 expressing EV or ZBTB18; cultured in either normal medium or lipid-depleted medium for 48 hours) were plated at 50,000 cells/well and allowed to adhere overnight. Then, the medium was changed over to Seahorse XF DMEM base medium, without phenol red (Agilent) supplemented with 10 mM Glucose , 2 mM Glutamine, and 1 mM Sodium Pyruvate pH 7.4. The metabolic parameters were measured using an ATP production rate assay kit by recording the basal values of OCR and ECAR for each condition and then the values after the injection of 1.5 μM oligomycin (final concentration) and of 0.5 μM rotenone /antimycin A (final). ATP produced from glycolysis was calculated as follows:

glycoATP Production Rate (pmol ATP/min) = glycoPER (pmol H^+/min);

ATP produced by mitochondrial respiration was calculated as follows:

1. OCR_{ATP} (pmol O_2/min) = OCR (pmol O_2/min) - $OCR_{Oligomycin}$ (pmol O2/min)
2. mitoATP Production Rate (pmol ATP/min) = OCR_{ATP} (pmol O_2/min) * 2 (pmol O/pmol O_2) * P/O (pmol ATP/pmol O);

Finally, total ATP production was calculated as follows:

ATP Production Rate (pmol ATP/min) = glycoATP Production Rate (pmol ATP/min) + mitoATP Production Rate (pmol ATP/min).

Statistical analysis

For the statistical analysis of the RT-qPCR data are judged to be statistically significant when $p < 0.05$ by two-tailed Student's t test. The number of replicates is indicated in each Figure legends.

REFERENCES

1. Ostrom QT, Gittleman H, Fulop J, Liu M, Blanda R, Kromer C*, et al.* CBTRUS Statistical Report: Primary Brain and Central Nervous System Tumors Diagnosed in the United States in 2008-2012. Neuro-oncology **2015**;17 Suppl 4:iv1-iv62 doi 10.1093/neuonc/nov189.
2. Wang J, Cazzato E, Ladewig E, Frattini V, Rosenbloom DI, Zairis S*, et al.* Clonal evolution of glioblastoma under therapy. Nature genetics **2016**;48(7):768-76 doi 10.1038/ng.3590.
3. Phillips HS, Kharbanda S, Chen R, Forrest WF, Soriano RH, Wu TD*, et al.* Molecular subclasses of high-grade glioma predict prognosis, delineate a pattern of disease progression, and resemble stages in neurogenesis. Cancer Cell **2006**;9(3):157-73 doi S1535-6108(06)00056-0 [pii] 10.1016/j.ccr.2006.02.019.
4. Verhaak RG, Hoadley KA, Purdom E, Wang V, Qi Y, Wilkerson MD*, et al.* Integrated Genomic Analysis Identifies Clinically Relevant Subtypes of Glioblastoma Characterized by Abnormalities in PDGFRA, IDH1, EGFR, and NF1. Cancer Cell **2010**;17(1):98-110 doi S1535-6108(09)00432-2 [pii] 10.1016/j.ccr.2009.12.020.
5. Bhat KPL, Balasubramaniyan V, Vaillant B, Ezhilarasan R, Hummelink K, Hollingsworth F*, et al.* Mesenchymal differentiation mediated by NF-kappaB promotes radiation resistance in glioblastoma. Cancer Cell **2013**;24(3):331-46 doi 10.1016/j.ccr.2013.08.001.
6. Wang Q, Hu B, Hu X, Kim H, Squatrito M, Scarpace L*, et al.* Tumor Evolution of Glioma-Intrinsic Gene Expression Subtypes Associates with Immunological

Changes in the Microenvironment. Cancer Cell **2017**;32(1):42-56 e6 doi 10.1016/j.ccell.2017.06.003.
7. Fedele M, Cerchia L, Pegoraro S, Sgarra R, Manfioletti G. Proneural-Mesenchymal Transition: Phenotypic Plasticity to Acquire Multitherapy Resistance in Glioblastoma. International journal of molecular sciences **2019**;20(11) doi 10.3390/ijms20112746.
8. Cheng WY, Kandel JJ, Yamashiro DJ, Canoll P, Anastassiou D. A multi-cancer mesenchymal transition gene expression signature is associated with prolonged time to recurrence in glioblastoma. PLoS One **2012**;7(4):e34705 doi 10.1371/journal.pone.0034705.
9. Romani M, Pistillo MP, Banelli B. Epigenetic Targeting of Glioblastoma. Front Oncol **2018**;8:448 doi 10.3389/fonc.2018.00448.
10. Kim TW, Kang BH, Jang H, Kwak S, Shin J, Kim H*, et al.* Ctbp2 Modulates NuRD-Mediated Deacetylation of H3K27 and Facilitates PRC2-Mediated H3K27me3 in Active Embryonic Stem Cell Genes During Exit from Pluripotency. Stem Cells **2015**;33(8):2442-55 doi 10.1002/stem.2046.
11. Ray SK, Li HJ, Metzger E, Schule R, Leiter AB. CtBP and associated LSD1 are required for transcriptional activation by NeuroD1 in gastrointestinal endocrine cells. Molecular and cellular biology **2014**;34(12):2308-17 doi 10.1128/MCB.01600-13.
12. Shi Y, Sawada J, Sui G, Affar el B, Whetstine JR, Lan F*, et al.* Coordinated histone modifications mediated by a CtBP co-repressor complex. Nature **2003**;422(6933):735-8 doi 10.1038/nature01550.
13. Boxer LD, Barajas B, Tao S, Zhang J, Khavari PA. ZNF750 interacts with KLF4 and RCOR1, KDM1A, and CTBP1/2 chromatin regulators to repress epidermal progenitor genes and induce differentiation genes. Genes & development **2014**;28(18):2013-26 doi 10.1101/gad.246579.114.
14. Bajpe PK, Heynen GJ, Mittempergher L, Grernrum W, de Rink IA, Nijkamp W*, et al.* The corepressor CTBP2 is a coactivator of retinoic acid receptor/retinoid X receptor in retinoic acid signaling. Molecular and cellular biology **2013**;33(16):3343-53 doi 10.1128/MCB.01213-12.
15. Di LJ, Byun JS, Wong MM, Wakano C, Taylor T, Bilke S*, et al.* Genome-wide profiles of CtBP link metabolism with genome stability and epithelial reprogramming in breast cancer. Nature communications **2013**;4:1449 doi 10.1038/ncomms2438.
16. Wang Y, Che S, Cai G, He Y, Chen J, Xu W. Expression and prognostic significance of CTBP2 in human gliomas. Oncology letters **2016**;12(4):2429-34 doi 10.3892/ol.2016.4998.
17. Horton JD, Goldstein JL, Brown MS. SREBPs: activators of the complete program of cholesterol and fatty acid synthesis in the liver. The Journal of clinical investigation **2002**;109(9):1125-31 doi 10.1172/JCI15593.
18. Horton JD, Shah NA, Warrington JA, Anderson NN, Park SW, Brown MS*, et al.* Combined analysis of oligonucleotide microarray data from transgenic and knockout mice identifies direct SREBP target genes. Proceedings of the National Academy of Sciences of the United States of America **2003**;100(21):12027-32 doi 10.1073/pnas.1534923100.

19. Lewis CA, Brault C, Peck B, Bensaad K, Griffiths B, Mitter R*, et al.* SREBP maintains lipid biosynthesis and viability of cancer cells under lipid- and oxygen-deprived conditions and defines a gene signature associated with poor survival in glioblastoma multiforme. Oncogene **2015**;34(40):5128-40 doi 10.1038/onc.2014.439.
20. Bensaad K, Favaro E, Lewis CA, Peck B, Lord S, Collins JM*, et al.* Fatty acid uptake and lipid storage induced by HIF-1alpha contribute to cell growth and survival after hypoxia-reoxygenation. Cell reports **2014**;9(1):349-65 doi 10.1016/j.celrep.2014.08.056.
21. Yue S, Li J, Lee SY, Lee HJ, Shao T, Song B*, et al.* Cholesteryl ester accumulation induced by PTEN loss and PI3K/AKT activation underlies human prostate cancer aggressiveness. Cell Metab **2014**;19(3):393-406 doi 10.1016/j.cmet.2014.01.019.
22. Currie E, Schulze A, Zechner R, Walther TC, Farese RV, Jr. Cellular fatty acid metabolism and cancer. Cell Metab **2013**;18(2):153-61 doi 10.1016/j.cmet.2013.05.017.
23. Menendez JA, Lupu R. Fatty acid synthase and the lipogenic phenotype in cancer pathogenesis. Nature reviews Cancer **2007**;7(10):763-77 doi 10.1038/nrc2222.
24. Guo D, Reinitz F, Youssef M, Hong C, Nathanson D, Akhavan D*, et al.* An LXR agonist promotes glioblastoma cell death through inhibition of an EGFR/AKT/SREBP-1/LDLR-dependent pathway. Cancer discovery **2011**;1(5):442-56 doi 10.1158/2159-8290.CD-11-0102.
25. Geng F, Cheng X, Wu X, Yoo JY, Cheng C, Guo JY*, et al.* Inhibition of SOAT1 Suppresses Glioblastoma Growth via Blocking SREBP-1-Mediated Lipogenesis. Clinical cancer research : an official journal of the American Association for Cancer Research **2016**;22(21):5337-48 doi 10.1158/1078-0432.CCR-15-2973.
26. Carro MS, Lim WK, Alvarez MJ, Bollo RJ, Zhao X, Snyder EY*, et al.* The transcriptional network for mesenchymal transformation of brain tumours. Nature **2010**;463(7279):318-25 doi nature08712 [pii] 10.1038/nature08712.
27. Fedele V, Dai F, Masilamani A, Heiland DH, Kling E, Gatjens-Sanchez A*, et al.* Epigenetic Regulation of ZBTB18 Promotes Glioblastoma Progression. Mol Cancer Res **2017** doi 10.1158/1541-7786.MCR-16-0494.
28. Dai F, Xuan Y, Jin JJ, Yu S, Long ZW, Cai H*, et al.* CtBP2 overexpression promotes tumor cell proliferation and invasion in gastric cancer and is associated with poor prognosis. Oncotarget **2017**;8(17):28736-49 doi 10.18632/oncotarget.15661.
29. Paliwal S, Ho N, Parker D, Grossman SR. CtBP2 Promotes Human Cancer Cell Migration by Transcriptional Activation of Tiam1. Genes & cancer **2012**;3(7-8):481-90 doi 10.1177/1947601912463695.
30. Yang X, Sun Y, Li H, Shao Y, Zhao D, Yu W*, et al.* C-terminal binding protein-2 promotes cell proliferation and migration in breast cancer via suppression of p16INK4A. Oncotarget **2017**;8(16):26154-68 doi 10.18632/oncotarget.15402.
31. Nibu Y, Levine MS. CtBP-dependent activities of the short-range Giant repressor in the Drosophila embryo. Proceedings of the National Academy of Sciences of the United States of America **2001**;98(11):6204-8 doi 10.1073/pnas.111158298.

32. Kucharczak J, Pannequin J, Camby I, Decaestecker C, Kiss R, Martinez J. Gastrin induces over-expression of genes involved in human U373 glioblastoma cell migration. Oncogene **2001**;20(48):7021-8 doi 10.1038/sj.onc.1204882.
33. Camby I, Belot N, Lefranc F, Sadeghi N, de Launoit Y, Kaltner H*, et al.* Galectin-1 modulates human glioblastoma cell migration into the brain through modifications to the actin cytoskeleton and levels of expression of small GTPases. Journal of neuropathology and experimental neurology **2002**;61(7):585-96 doi 10.1093/jnen/61.7.585.
34. Zheng X, Song T, Dou C, Jia Y, Liu Q. CtBP2 is an independent prognostic marker that promotes GLI1 induced epithelial-mesenchymal transition in hepatocellular carcinoma. Oncotarget **2015**;6(6):3752-69 doi 10.18632/oncotarget.2915.
35. Wang Y, Wang H, Zhao Q, Xia Y, Hu X, Guo J. PD-L1 induces epithelial-to-mesenchymal transition via activating SREBP-1c in renal cell carcinoma. Medical oncology **2015**;32(8):212 doi 10.1007/s12032-015-0655-2.
36. Yang L, Yang J, Li J, Shen X, Le Y, Zhou C*, et al.* MircoRNA-33a inhibits epithelial-to-mesenchymal transition and metastasis and could be a prognostic marker in non-small cell lung cancer. Scientific reports **2015**;5:13677 doi 10.1038/srep13677.
37. Bowman RL, Wang Q, Carro A, Verhaak RG, Squatrito M. GlioVis data portal for visualization and analysis of brain tumor expression datasets. Neuro-oncology **2017**;19(1):139-41 doi 10.1093/neuonc/now247.
38. Achouri Y, Noel G, Van Schaftingen E. 2-Keto-4-methylthiobutyrate, an intermediate in the methionine salvage pathway, is a good substrate for CtBP1. Biochemical and biophysical research communications **2007**;352(4):903-6 doi 10.1016/j.bbrc.2006.11.111.
39. Zhao Z, Meng F, Wang W, Wang Z, Zhang C, Jiang T. Comprehensive RNA-seq transcriptomic profiling in the malignant progression of gliomas. Sci Data **2017**;4:170024 doi 10.1038/sdata.2017.24.
40. Cheneby J, Menetrier Z, Mestdagh M, Rosnet T, Douida A, Rhalloussi W*, et al.* ReMap 2020: a database of regulatory regions from an integrative analysis of Human and Arabidopsis DNA-binding sequencing experiments. Nucleic Acids Res **2019** doi 10.1093/nar/gkz945.
41. Hublitz P, Albert M, Peters AH. Mechanisms of transcriptional repression by histone lysine methylation. Int J Dev Biol **2009**;53(2-3):335-54 doi 10.1387/ijdb.082717ph.
42. Deltour S, Pinte S, Guerardel C, Wasylyk B, Leprince D. The human candidate tumor suppressor gene HIC1 recruits CtBP through a degenerate GLDLSKK motif. Molecular and cellular biology **2002**;22(13):4890-901.
43. Metzger E, Wissmann M, Yin N, Muller JM, Schneider R, Peters AH*, et al.* LSD1 demethylates repressive histone marks to promote androgen-receptor-dependent transcription. Nature **2005**;437(7057):436-9 doi 10.1038/nature04020.
44. Shi Y, Lan F, Matson C, Mulligan P, Whetstine JR, Cole PA*, et al.* Histone demethylation mediated by the nuclear amine oxidase homolog LSD1. Cell **2004**;119(7):941-53 doi 10.1016/j.cell.2004.12.012.
45. Roder K, Schweizer M. Retinoic acid-mediated transcription and maturation of SREBP-1c regulates fatty acid synthase via cis-elements responsible for

nutritional regulation. Biochem Soc Trans **2007**;35(Pt 5):1211-4 doi 10.1042/BST0351211.
46. Costet P, Lalanne F, Gerbod-Giannone MC, Molina JR, Fu X, Lund EG*, et al.* Retinoic acid receptor-mediated induction of ABCA1 in macrophages. Molecular and cellular biology **2003**;23(21):7756-66 doi 10.1128/mcb.23.21.7756-7766.2003.
47. Abdulla A, Zhang Y, Hsu FN, Xiaoli AM, Zhao X, Yang ES*, et al.* Regulation of lipogenic gene expression by lysine-specific histone demethylase-1 (LSD1). The Journal of biological chemistry **2014**;289(43):29937-47 doi 10.1074/jbc.M114.573659.
48. Chen M, Zhu N, Liu X, Laurent B, Tang Z, Eng R*, et al.* JMJD1C is required for the survival of acute myeloid leukemia by functioning as a coactivator for key transcription factors. Genes & development **2015**;29(20):2123-39 doi 10.1101/gad.267278.115.
49. Salzberg AC, Harris-Becker A, Popova EY, Keasey N, Loughran TP, Claxton DF*, et al.* Genome-wide mapping of histone H3K9me2 in acute myeloid leukemia reveals large chromosomal domains associated with massive gene silencing and sites of genome instability. PLoS One **2017**;12(3):e0173723 doi 10.1371/journal.pone.0173723.
50. Schulte JH, Lim S, Schramm A, Friedrichs N, Koster J, Versteeg R*, et al.* Lysine-specific demethylase 1 is strongly expressed in poorly differentiated neuroblastoma: implications for therapy. Cancer Res **2009**;69(5):2065-71 doi 10.1158/0008-5472.CAN-08-1735.
51. Zhao Z, Hao D, Wang L, Li J, Meng Y, Li P*, et al.* CtBP promotes metastasis of breast cancer through repressing cholesterol and activating TGF-beta signaling. Oncogene **2019**;38(12):2076-91 doi 10.1038/s41388-018-0570-z.
52. Kuhajda FP, Pizer ES, Li JN, Mani NS, Frehywot GL, Townsend CA. Synthesis and antitumor activity of an inhibitor of fatty acid synthase. Proceedings of the National Academy of Sciences of the United States of America **2000**;97(7):3450-4 doi 10.1073/pnas.050582897.
53. Gopal K, Grossi E, Paoletti P, Usardi M. Lipid Composition of Human Intracranial Tumors: A Biochemical Study. Acta neurochirurgica **1963**;11:333-47 doi 10.1007/bf01402012.
54. Srivastava NK, Pradhan S, Gowda GA, Kumar R. In vitro, high-resolution 1H and 31P NMR based analysis of the lipid components in the tissue, serum, and CSF of the patients with primary brain tumors: one possible diagnostic view. NMR Biomed **2010**;23(2):113-22 doi 10.1002/nbm.1427.
55. Cohen P, Miyazaki M, Socci ND, Hagge-Greenberg A, Liedtke W, Soukas AA*, et al.* Role for stearoyl-CoA desaturase-1 in leptin-mediated weight loss. Science **2002**;297(5579):240-3 doi 10.1126/science.1071527.
56. Miyazaki M, Flowers MT, Sampath H, Chu K, Otzelberger C, Liu X*, et al.* Hepatic stearoyl-CoA desaturase-1 deficiency protects mice from carbohydrate-induced adiposity and hepatic steatosis. Cell Metab **2007**;6(6):484-96 doi 10.1016/j.cmet.2007.10.014.
57. Olzmann JA, Carvalho P. Dynamics and functions of lipid droplets. Nature reviews Molecular cell biology **2019**;20(3):137-55 doi 10.1038/s41580-018-0085-z.

58. Duman C, Yaqubi K, Hoffmann A, Acikgoz AA, Korshunov A, Bendszus M*, et al.* Acyl-CoA-Binding Protein Drives Glioblastoma Tumorigenesis by Sustaining Fatty Acid Oxidation. Cell Metab **2019**;30(2):274-89 e5 doi 10.1016/j.cmet.2019.04.004.
59. Guillou H, Zadravec D, Martin PG, Jacobsson A. The key roles of elongases and desaturases in mammalian fatty acid metabolism: Insights from transgenic mice. Prog Lipid Res **2010**;49(2):186-99 doi 10.1016/j.plipres.2009.12.002.
60. Xie Y, Bergstrom T, Jiang Y, Johansson P, Marinescu VD, Lindberg N*, et al.* The Human Glioblastoma Cell Culture Resource: Validated Cell Models Representing All Molecular Subtypes. EBioMedicine **2015**;2(10):1351-63 doi 10.1016/j.ebiom.2015.08.026.
61. Ritchie ME, Phipson B, Wu D, Hu Y, Law CW, Shi W*, et al.* limma powers differential expression analyses for RNA-sequencing and microarray studies. Nucleic Acids Res **2015**;43(7):e47 doi 10.1093/nar/gkv007.
62. Kamburov A, Stelzl U, Lehrach H, Herwig R. The ConsensusPathDB interaction database: 2013 update. Nucleic Acids Res **2013**;41(Database issue):D793-800 doi 10.1093/nar/gks1055.
63. Goldmann T, Zeller N, Raasch J, Kierdorf K, Frenzel K, Ketscher L*, et al.* USP18 lack in microglia causes destructive interferonopathy of the mouse brain. The EMBO journal **2015**;34(12):1612-29 doi 10.15252/embj.201490791.
64. Tucci S, Mingirulli N, Wehbe Z, Dumit VI, Kirschner J, Spiekerkoetter U. Mitochondrial fatty acid biosynthesis and muscle fiber plasticity in very long-chain acyl-CoA dehydrogenase-deficient mice. FEBS letters **2018**;592(2):219-32 doi 10.1002/1873-3468.12940.
65. Orchard S, Ammari M, Aranda B, Breuza L, Briganti L, Broackes-Carter F*, et al.* The MIntAct project--IntAct as a common curation platform for 11 molecular interaction databases. Nucleic Acids Res **2014**;42(Database issue):D358-63 doi 10.1093/nar/gkt1115.
66. Zhu LJ, Gazin C, Lawson ND, Pages H, Lin SM, Lapointe DS*, et al.* ChIPpeakAnno: a Bioconductor package to annotate ChIP-seq and ChIP-chip data. BMC bioinformatics **2010**;11:237 doi 10.1186/1471-2105-11-237.
67. Yu G, Wang LG, He QY. ChIPseeker: an R/Bioconductor package for ChIP peak annotation, comparison and visualization. Bioinformatics **2015**;31(14):2382-3 doi 10.1093/bioinformatics/btv145.
68. Lagies S, Pichler R, Kaminski MM, Schlimpert M, Walz G, Lienkamp SS*, et al.* Metabolic characterization of directly reprogrammed renal tubular epithelial cells (iRECs). Scientific reports **2018**;8(1):3878 doi 10.1038/s41598-018-22073-7.
69. Sapcariu SC, Kanashova T, Weindl D, Ghelfi J, Dittmar G, Hiller K. Simultaneous extraction of proteins and metabolites from cells in culture. MethodsX **2014**;1:74-80 doi 10.1016/j.mex.2014.07.002.
70. Chong J, Soufan O, Li C, Caraus I, Li S, Bourque G*, et al.* MetaboAnalyst 4.0: towards more transparent and integrative metabolomics analysis. Nucleic Acids Res **2018**;46(W1):W486-W94 doi 10.1093/nar/gky310.

FIGURE LEGENDS

Fig. 1. ZBTB18 interacts with CTBP2 through the VLDLS domain in glioblastoma cells. A Coomassie staining analysis of FLAG-ZBTB18 co-IP in SNB19 GBM cells transduced with EV or FLAG-ZBTB18. **B** List of ZBTB18 co-precipitated proteins. **C** Western blot analysis of FLAG and ZBTB18 co-IPs in SNB19 cells using anti-ZBTB18 and anti-CTBP2 antibodies. **D** Western blot analysis of FLAG and CTBP2 co-IPs in SNB19 cells using anti-FLAG and anti-CTBP2 antibodies. **E** Schematic representation of ZBTB18 protein with BTB and Zinc fingers domain. The putative CTBP2 interacting motif (VLDLS) and corresponding mutation are marked. **F** Western blot analysis of FLAG co-IP in SNB19 cells expressing either ZBTB18 or ZBTB18-mut, using anti-FLAG and anti-CTBP2 antibodies. **G** Western blot analysis of CTBP2 co-IP in SNB19 cells expressing either ZBTB18 or ZBTB18-mut, using anti-ZBTB18 and anti-CTBP2 antibodies. **H** qRT-PCR showing expression of ZBTB18 targets upon ZBTB18 and ZBTB18-mut overexpression in SNB19 cells. n=3; error bars ± s.d. *$p < 0.05$, **$p < 0.01$, ***$p < 0.001$. Gene expression was normalized to 18sRNA.

Fig. 2. ZBTB18 and CTBP2 regulate the expression of SREBP genes involved in fatty acid synthesis. A Western blot analysis of FLAG-ZBTB18 and CTBP2 expression in SNB19 cells transduced with either FLAG-ZBTB18 or shCTBP2. **B** Venn analysis showing the overlap between regulated genes in ZBTB18 vs. EV and genes regulated in shCTBP2 vs. shCtr (upper part) or ZBTB18 shCTBP2 vs. EV (lower part). Genes where selected based on adjusted p value < 0.05 and absolute fold change > 0.5. **C** Top 10 downregulated consensus pathways in the overlap between shCTBP2 vs. shCtr and ZBTB18 vs. EV regulated genes (ZBTB18 vs shCTBP2) from Fisher's exact test comparing the DEGs (adj. p value < 0.05, FC < -0.5) to the whole set of quantified

genes. Processes related to SREBP signaling are highlighted. **D** Row-wise z-score heatmap showing the expression of SREBP signaling genes in each triplicate across the 4 conditions, i.e. EV shCtr, EV shCTBP2, ZBTB18 shCTBP2 and ZBTB18 shCtr. Rows and columns hierarchical clustering are both based on Euclidean distance and complete clustering method was used. **E** q-RT PCR validation of selected SREBP genes expression upon ZBTB18 expression and/or CTBP2 silencing. n=3; error bars ± s.d. *p < 0.05, **p < 0.01, ***p < 0.001. Gene expression was normalized to 18s RNA. **F** q-RT PCR analysis of selected SREBP genes in SNB19 cells treated with the CTBP2 inhibitor MTOB. n=3; error bars ± s.d. *p < 0.05, **p < 0.01, ***p < 0.001. Gene expression was normalized to 18s RNA. **G** Representative q-RT PCR analysis of selected SREBP genes, upon ZBTB18 overexpression and MTOB treatment. Error bars ± s.d. Gene expression was normalized to 18s RNA. **H** Representative q-RT PCR analysis of selected SREBP gene expression, upon ZBTB18 or ZBTB18-mut expression. n=3 PCR replicates; error bars ± s.d. Gene expression was normalized to 18s RNA. **I** Kaplan-Meier curve showing survival of mice injected with shCTBP2-transduced SNB19 cells (n=7) compared with the respective control (SNB19-shCtr, n=9). **J** Table summarizing the number of tumors and median survival of the injected mice. **K** Representative images of mouse brains bearing tumors derived from shCtr or shCTBP2-transduced SNB19 cells. Scale bar indicates 1mm.

Fig. 3. CTBP2 and ZBTB18 map to SREBP gene promoters. A Experimental flow chart of the ChIP sequencing analysis. **B** Venn diagram showing the overlap between the 3 consensus peak sets from EV_CTBP2, ZBTB18_CTBP2 and ZBTB18_FLAG. The percentage of overlap is indicated in red. **C** Enrichment of peaks on promoter regions depicted on a forest plot from Fisher's test analysis. Identified peaks were compared

against 100 000 randomly chosen regions of 200bp over the entire genome. Dots indicate the Odd ratio and lines indicate the 95% confidence interval. **D** Meta-gene peak density profile showing an over-representation of peaks around SREBP genes TSS regions. Y-axis indicates the percentage of peaks in each group that overlap the genomic region depicted on the X-axis. **E** UpSet plot showing the overlap of SREBP genes having at least one peak in one of the 3 conditions: EV_CTBP2, ZBTB18_CTBP2 and ZBTB18_FLAG. **F** Read coverage around biological relevant selected genes, i.e. FASN, GSK3A, INSIG1, SCAP and SCD. Identified peaks are highlighted under the grey area and genes TSS are drawn on top of the plot. **G-H** FLAG-ZBTB18 (**G**) and CTBP2 (**H**) enrichment at the promoter of the indicated SREBP genes in SNB19 cells transduced with the empty vector (EV) or the vector expressing FLAG-ZBTB18 (ZBTB18). ChIP was performed using control beads alone (IgG), anti-FLAG antibodies or anti-CTBP2 antibody. Graphs show qPCR results expressed in % input as indicated.

Fig. 4. ZBTB18 recruits CTBP2 complex to the promoter of SREBP genes. ZBTB18 recruits CTBP2 complex to the promoter of SREBP genes. **A** Experimental flow chart of the SILAC-based MS analysis. **B** List of known CTBP2 interacting proteins identified by SILAC. Binding to CTBP2 increases in the presence of ZBTB18 (H) respect to EV (L). **C** Left panel: validation of SILAC results by co-IP with anti CTBP2 antibody. Binding of ZNF217 and LSD1 to CTBP2 is increased or stabilized in presence of ZBTB18. Right panel: quantification of co-IP results. **D-G** qPCR showing binding of ZNF217 (**D**), LSD1 (**E**), H3K9me2 (**F**) and H3K4me3 (**G**) at selected SREBP gene promoters. ZNF217 and LSD1 binding increase in presence of ZBTB18. Increased presence of H3K9me2 indicates inhibition of LSD1 function. Decreased H3K4me3 is consistent with gene repression. **H-I** qPCR showing binding of LSD1 (**H**) and H3K9me2 (**I**), at selected

SREBP gene promoters in SNB19 cells transduced with EV, ZBTB18 and ZBTB18-mut. LSD1 and H3K9me2 are enriched in presence of ZBTB18 but not when ZBTB18-mut is expressed. **J** Bar chart showing LSD1 activity in SNB19 cells transduced with EV, ZBTB18, ZBTB18-mut (all n=7), or treated with the LSD1 inhibitor RN-1 (n=4). LSD1 activity is reduced upon ZBTB18 expression.

Fig. 5. ZBTB18 overexpression alters lipid content depending on its CTBP2 binding capability. A Experimental flow chart of lipidomics analysis. **B** Heatmap of significantly altered ($q < 0.05$) lipids in SNB19 cells expressing EV, ZBTB18 or ZBTB18-mut, grown in the presence (no suffix) or absence of lipids (NL). Range-scaled z-scores are displayed. **C** Bar charts showing the abundance of the significantly altered lipid species ($q < 0.05$) after normalizing the samples described in (**B**) to the corresponding EV condition. n=3; error bars ± s.d.

Fig. 6. ZBTB18 overexpression reduces lipid accumulation in the absence of an external supply. A Bodipy TMR-X lipid staining of SNB19 cells expressing EV, ZBTB18 or ZBTB18-mut, grown in lipid-containing medium (Normal medium), in conditions of lipid starvation (Lipid starvation) or in lipid-containing medium after a period of lipid starvation (Recovery). ZBTB18 was also immunolabeled and nuclei were counterstained with DAPI. Scale bar: 20µm. **B** Quantification of the lipid staining shown in (**A**). n=5; error bars ± s.d. *$p < 0.05$, **$p < 0.01$, ***$p < 0.001$. **C** Quantification of Bodipy-C16 uptake in SNB19 cells expressing EV, ZBTB18 or ZBTB18-mut. n=3; error bars ± s.d. *$p < 0.05$, **$p < 0.01$, ***$p < 0.001$.

Fig. 7. ZBTB18 overexpression reduces aerobic respiration in the absence of an external fatty acid supply. A Oxygen consumption rate (OCR) measured in a Seahorse ATP production rate assay in which oligomycin and rotenone/antimycin A

were added at given time points for each experiment. SNB19 cells expressing EV or ZBTB18, grown in lipid-containing medium or in conditions of lipid starvation were tested. n=5; error bars ± s.d. **B** Extracellular acidification rate (ECAR) measured in a Seahorse ATP production rate assay as described in (A). n=5; error bars ± s.d. **C** Stacked bar graph showing the glycolytic and mitochondrial contribution to the ATP production rate for the samples described in (A). n=5; error bars ± s.d. *$p < 0.05$, **$p < 0.01$, ***$p < 0.001$. **D** Graphical representation of the cell energy phenotype of the samples described in (A). n=5; error bars ± s.d. **E** Model of CTBP2 and ZBTB18-mediated transcriptional regulation of SREBP genes and effect on the cellular phenotype.

Figure 1

A

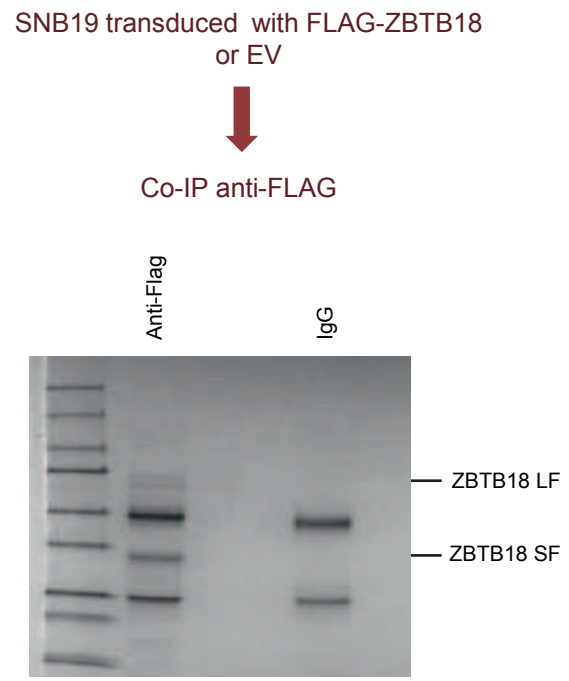

B

Gene names	Number of proteins	Peptides
HSPA5	1	27
HSPA8	16	22
CCT8	5	17
ZBTB18	1	17
CCT2	4	16
CCT6A	7	13
CCT5	6	13
TCP1	10	12
HSPA9	3	11
CCT3	6	9
PCMT1	10	8
HSPA1A	4	8
EEF1A1P5	5	8
PRDX1	2	7
CCT7	7	7
CCT4	4	6
PAICS	4	6
HSPA6	2	6
GSTP1	2	5
CTBP2	3	5
FLNA	4	4
CBR1	4	3
UBB	29	3
CBR3	1	3
DCD	2	3
CLTC	3	3
CTBP1	8	3
AMY2B	5	2

C

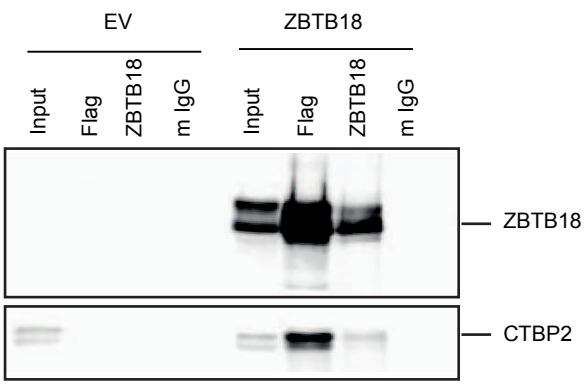

D

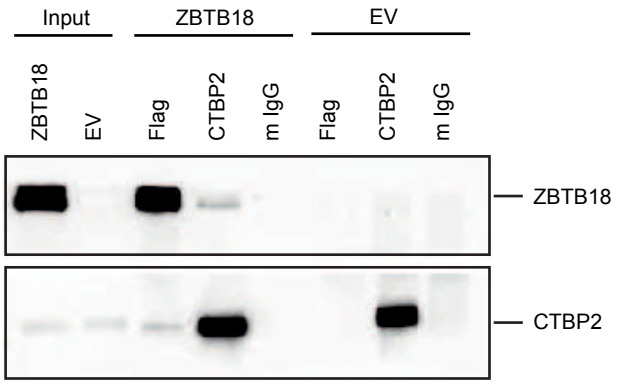

E

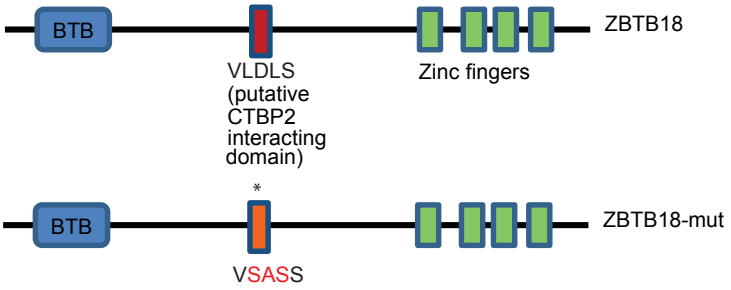

F

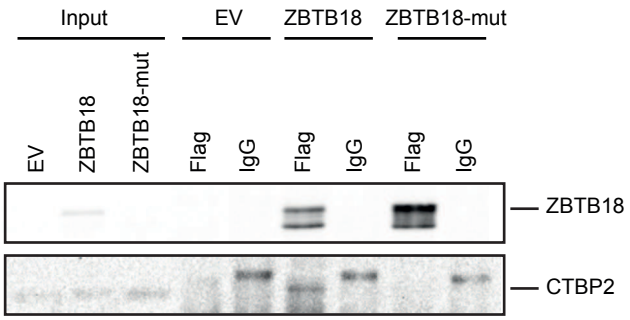

G

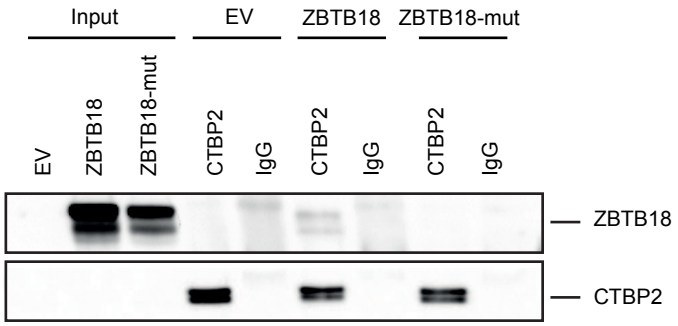

H

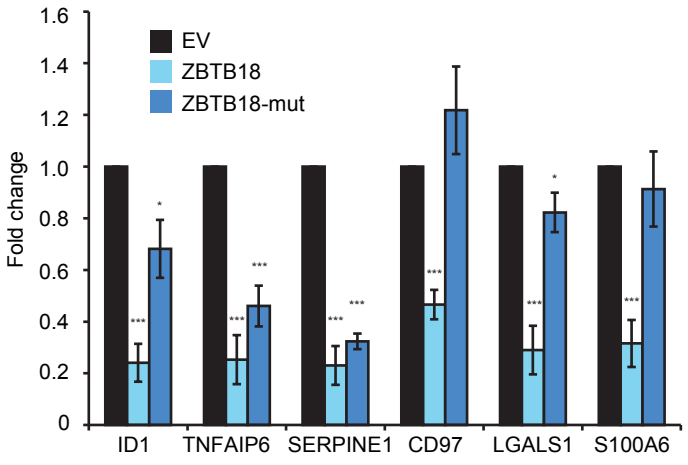

Figure 2

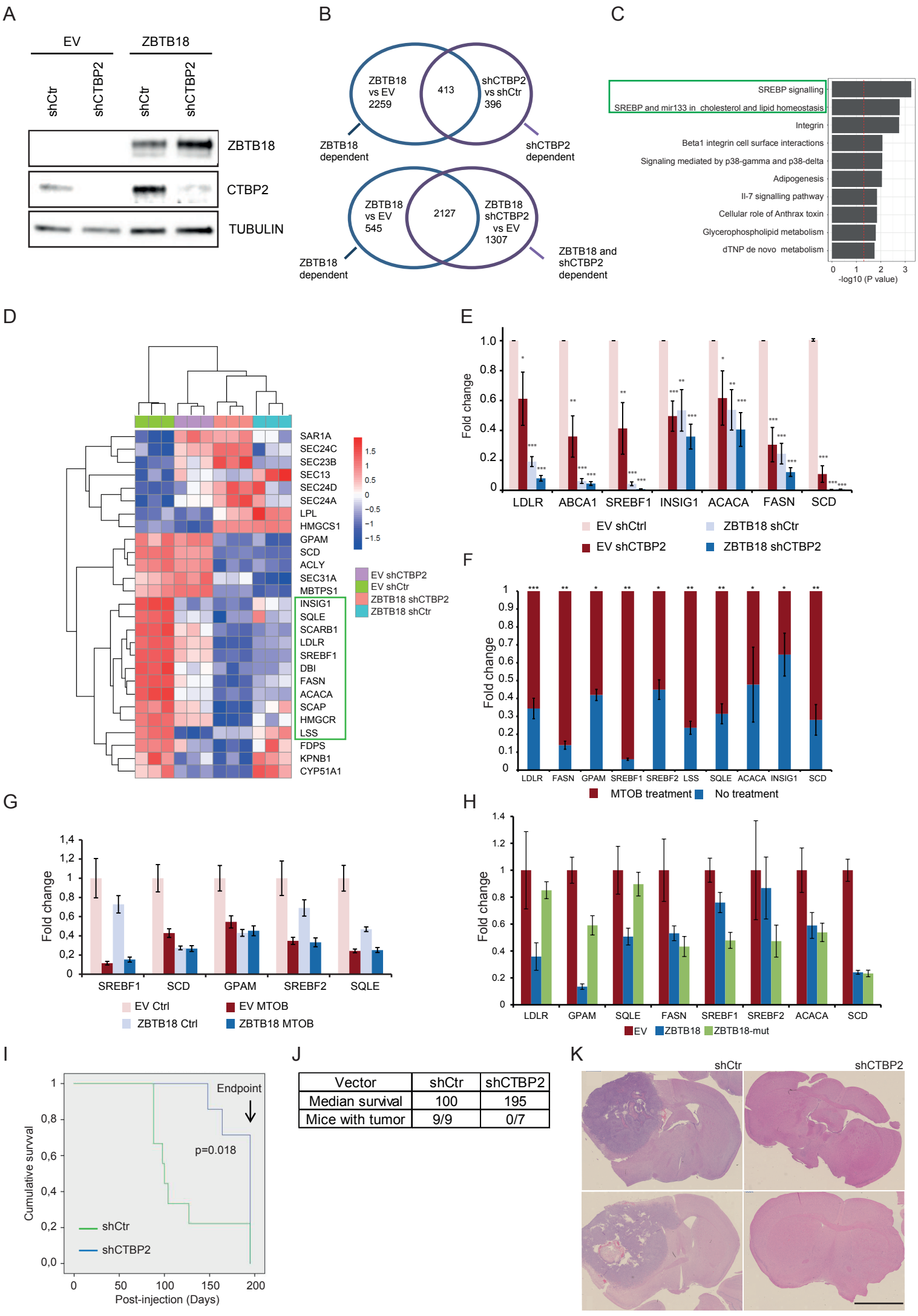

Vector	shCtr	shCTBP2
Median survival	100	195
Mice with tumor	9/9	0/7

Figure 3

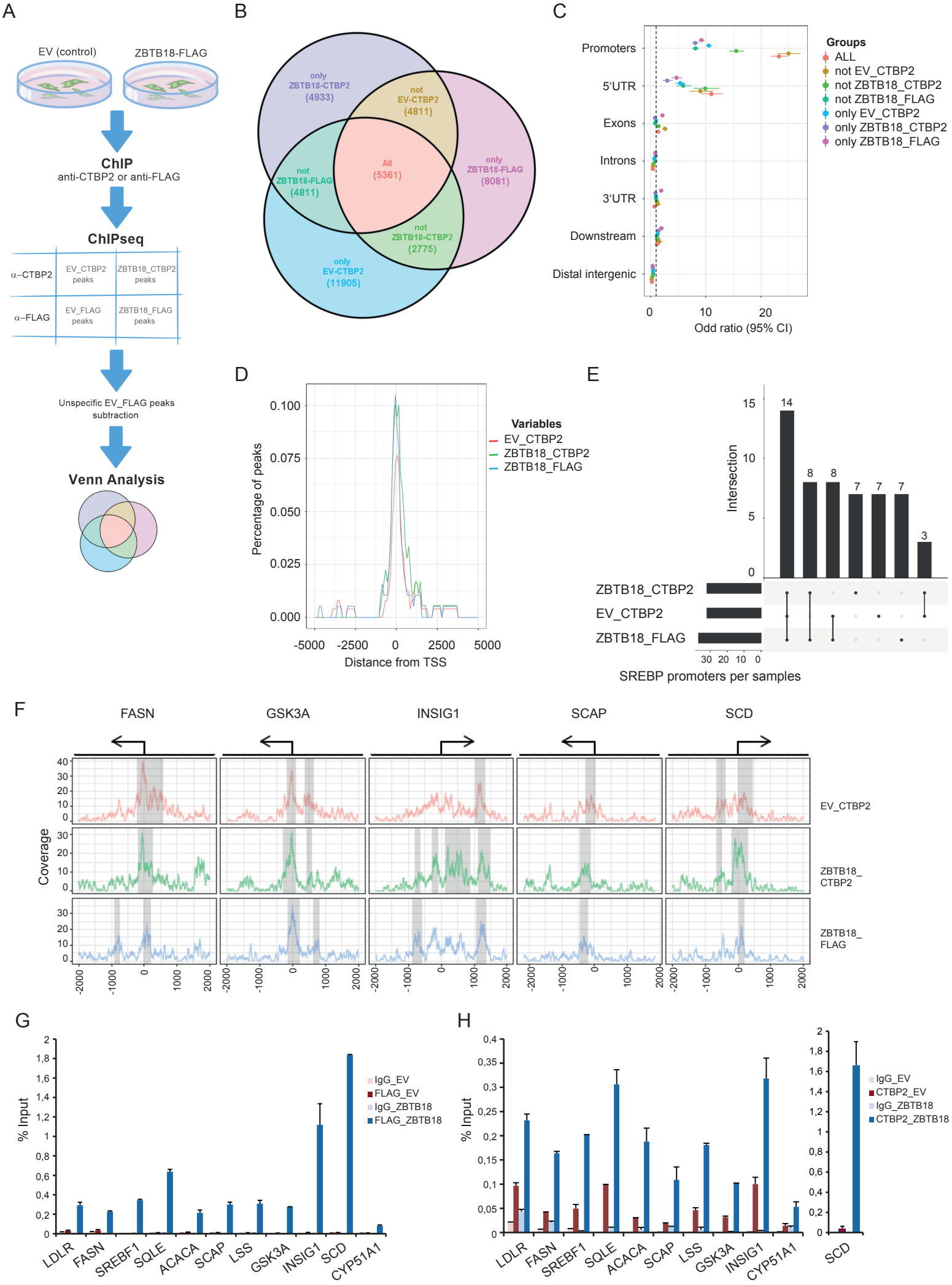
A
EV (control)
ZBTB18-FLAG
ChIP
anti-CTBP2 or anti-FLAG
ChIPseq
α–CTBP2
EV_CTBP2 peaks
ZBTB18_CTBP2 peaks
α–FLAG
EV_FLAG peaks
ZBTB18_FLAG peaks
Unspecific EV_FLAG peaks subtraction
Venn Analysis
B
only ZBTB18-CTBP2 (4933)
not EV-CTBP2 (4811)
All (5361)
not ZBTB18-FLAG (4811)
only ZBTB18-FLAG (8081)
not ZBTB18-CTBP2 (2775)
only EV-CTBP2 (11905)
C
Promoters
5'UTR
Exons
Introns
3'UTR
Downstream
Distal intergenic
Odd ratio (95% CI)
Groups
ALL
not EV_CTBP2
not ZBTB18_CTBP2
not ZBTB18_FLAG
only EV_CTBP2
only ZBTB18_CTBP2
only ZBTB18_FLAG
D
Percentage of peaks
Distance from TSS
Variables
EV_CTBP2
ZBTB18_CTBP2
ZBTB18_FLAG
E
Intersection
ZBTB18_CTBP2
EV_CTBP2
ZBTB18_FLAG
SREBP promoters per samples
F
FASN
GSK3A
INSIG1
SCAP
SCD
Coverage
EV_CTBP2
ZBTB18_CTBP2
ZBTB18_FLAG
G
% Input
IgG_EV
FLAG_EV
IgG_ZBTB18
FLAG_ZBTB18
LDLR
FASN
SREBF1
SQLE
ACACA
SCAP
LSS
GSK3A
INSIG1
SCD
CYP51A1
H
% Input
IgG_EV
CTBP2_EV
IgG_ZBTB18
CTBP2_ZBTB18

Figure 4

A

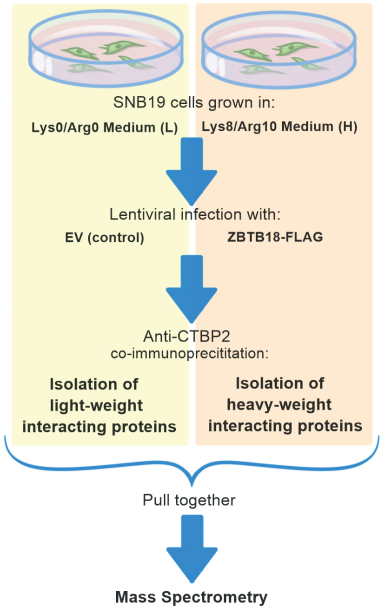

B

Gene names	Peptides	PEP	Ratio H/L	Ratio H/L normalized
ZNF217	6	1.07E-14	1.8348	1.6924
RCOR1	7	3.30E-35	1.7287	1.8255
LSD1/KDM1A	10	8.91E-69	1.592	1.6924
CTBP2	12	9.41E-297	1.5339	1.9103
HDAC1;HDAC2	3	1.32E-08	1.3482	1.4812
CTBP1	17	7.19E-260	1.1679	1.4637

C

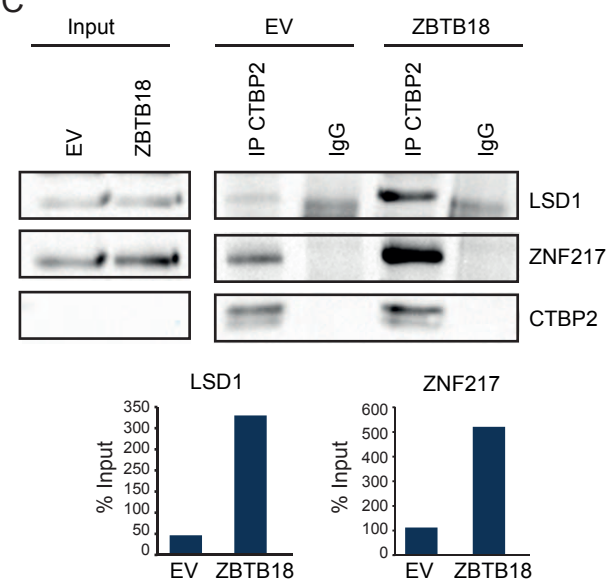

D

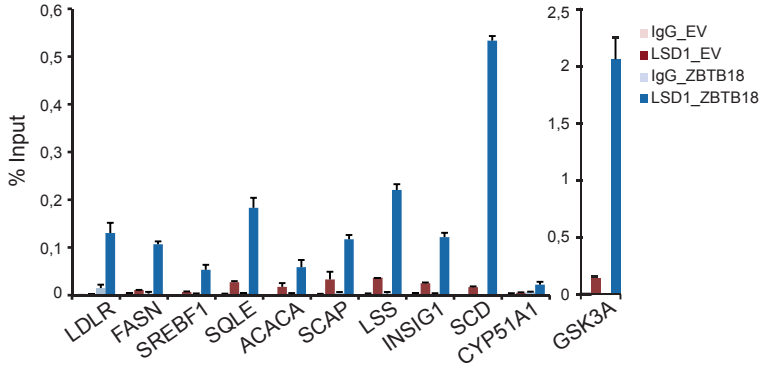

E

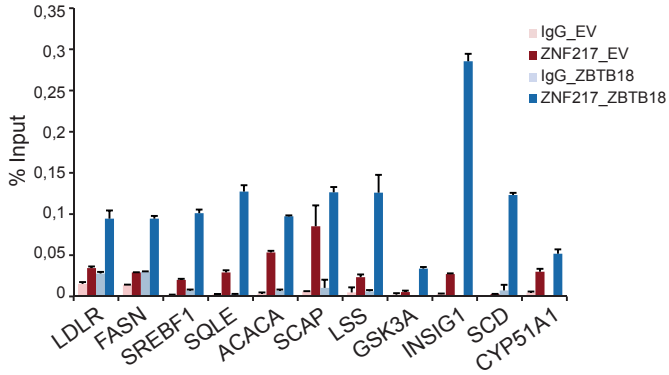

F

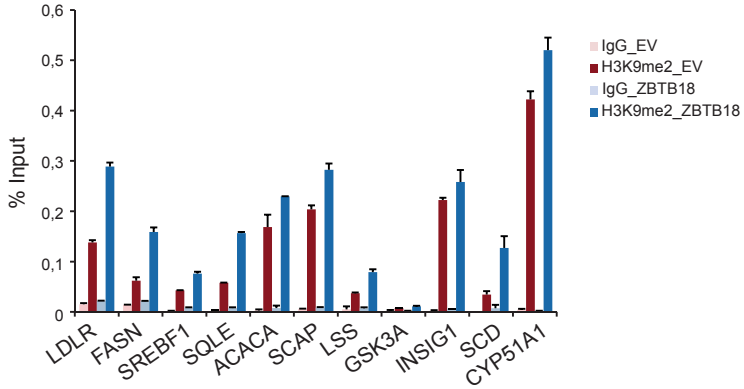

G

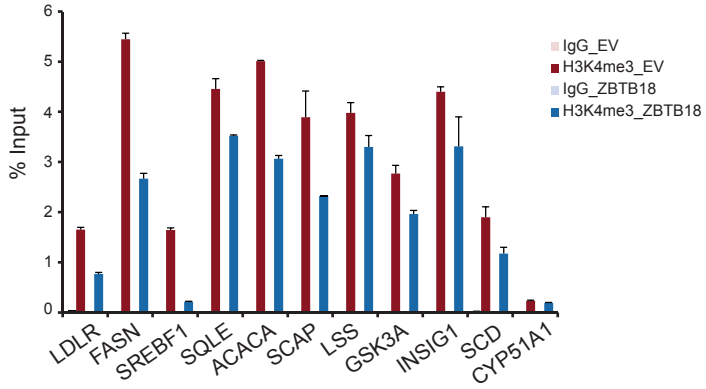

H

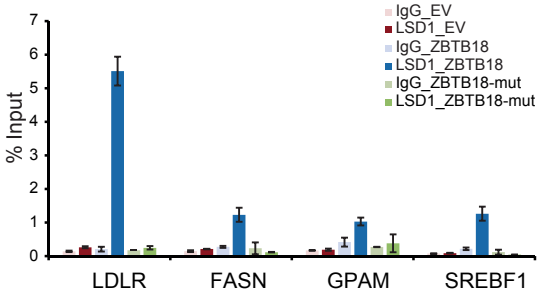

I

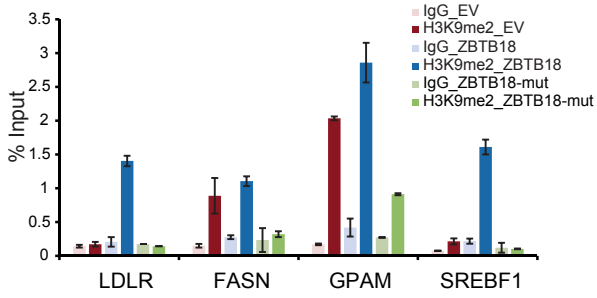

J

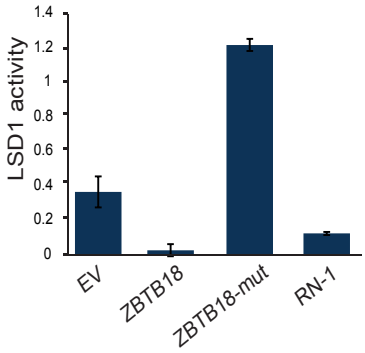

Figure 5

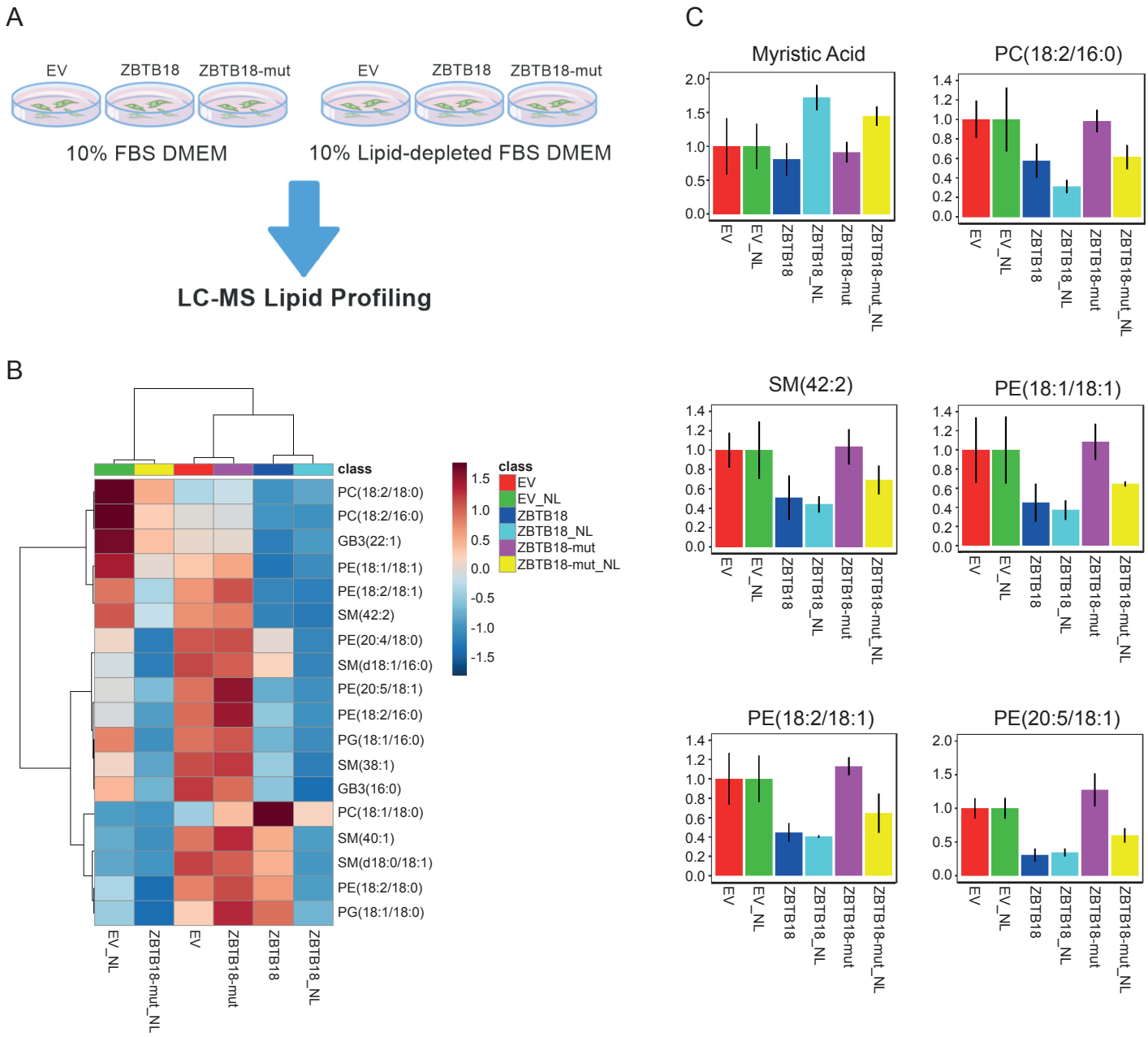
A
EV
ZBTB18
ZBTB18-mut
EV
ZBTB18
ZBTB18-mut
10% FBS DMEM
10% Lipid-depleted FBS DMEM
LC-MS Lipid Profiling
B
class
PC(18:2/18:0)
PC(18:2/16:0)
GB3(22:1)
PE(18:1/18:1)
PE(18:2/18:1)
SM(42:2)
PE(20:4/18:0)
SM(d18:1/16:0)
PE(20:5/18:1)
PE(18:2/16:0)
PG(18:1/16:0)
SM(38:1)
GB3(16:0)
PC(18:1/18:0)
SM(40:1)
SM(d18:0/18:1)
PE(18:2/18:0)
PG(18:1/18:0)
EV_NL
ZBTB18-mut_NL
EV
ZBTB18-mut
ZBTB18
ZBTB18_NL
1.5
1.0
0.5
0.0
-0.5
-1.0
-1.5
class
EV
EV_NL
ZBTB18
ZBTB18_NL
ZBTB18-mut
ZBTB18-mut_NL
C
Myristic Acid
PC(18:2/16:0)
SM(42:2)
PE(18:1/18:1)
PE(18:2/18:1)
PE(20:5/18:1)
EV
EV_NL
ZBTB18
ZBTB18_NL
ZBTB18-mut
ZBTB18-mut_NL

Figure 6

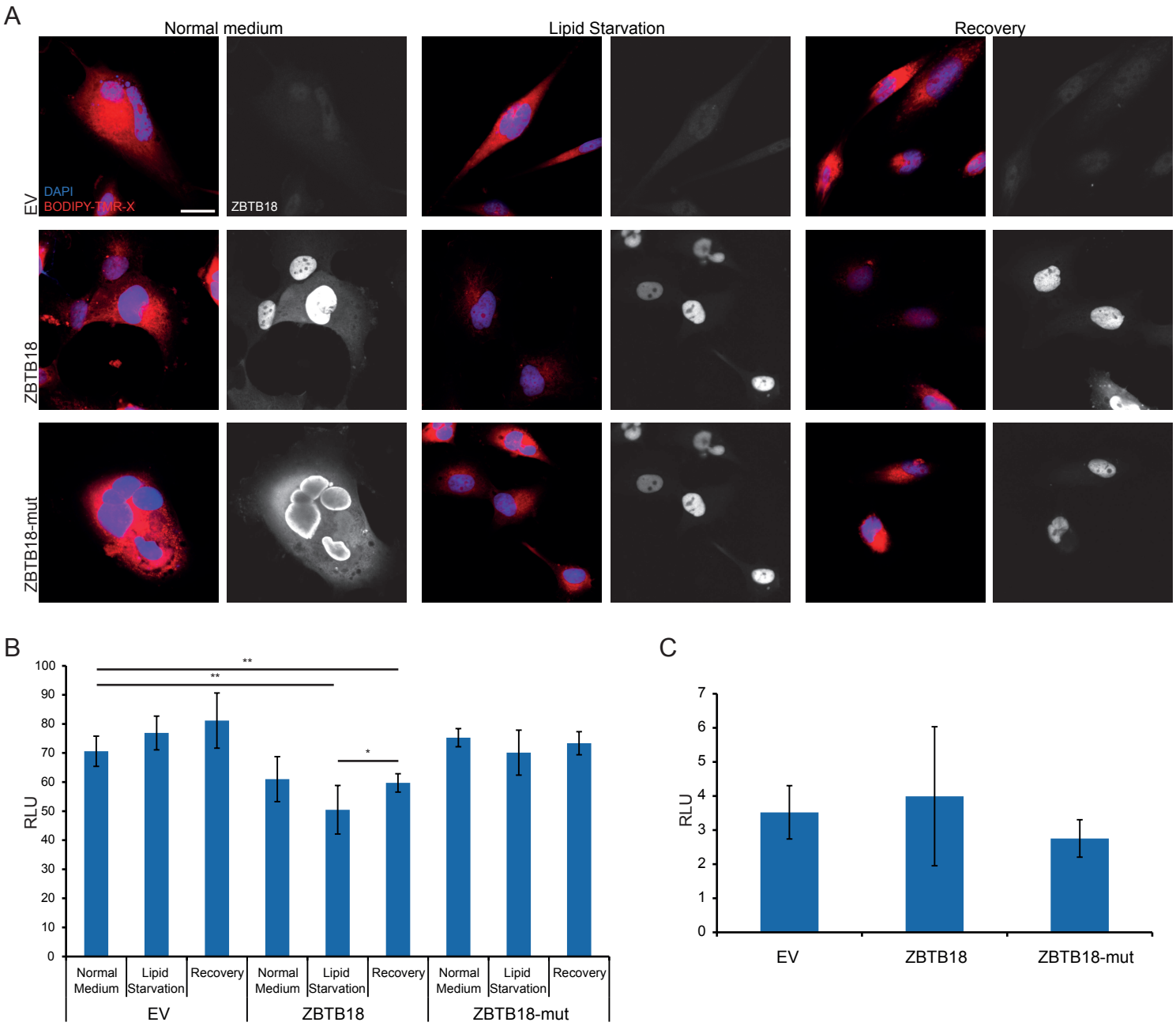
A
Normal medium
Lipid Starvation
Recovery
EV
ZBTB18
ZBTB18-mut
DAPI
BODIPY-TMR-X
ZBTB18
B
RLU
100
90
80
70
60
50
40
30
20
10
0
**
**
*
Normal Medium
Lipid Starvation
Recovery
Normal Medium
Lipid Starvation
Recovery
Normal Medium
Lipid Starvation
Recovery
EV
ZBTB18
ZBTB18-mut
C
RLU
7
6
5
4
3
2
1
0
EV
ZBTB18
ZBTB18-mut

Figure 7

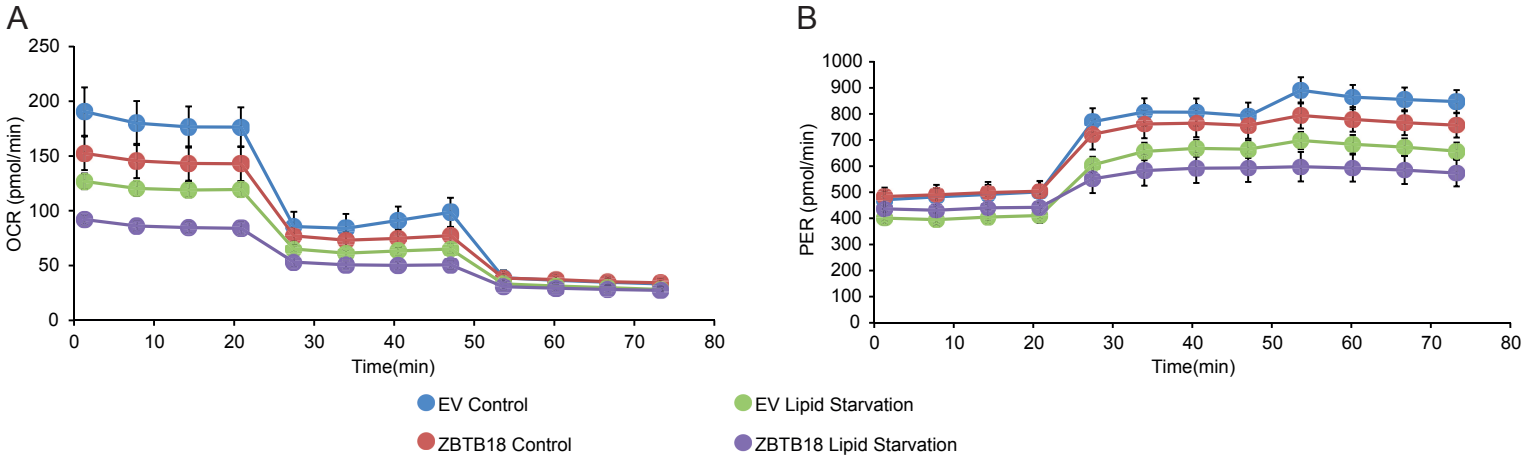
A
OCR (pmol/min)
Time(min)
B
PER (pmol/min)
Time(min)
EV Control
EV Lipid Starvation
ZBTB18 Control
ZBTB18 Lipid Starvation

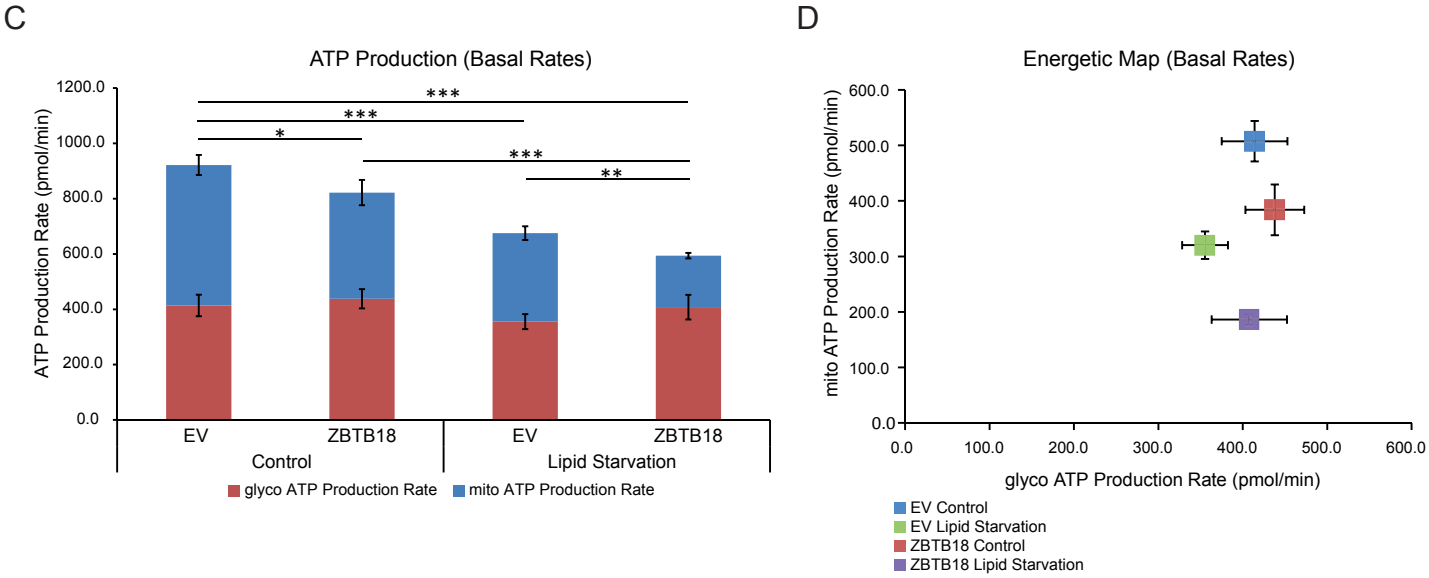
C
ATP Production (Basal Rates)
ATP Production Rate (pmol/min)
EV
ZBTB18
EV
ZBTB18
Control
Lipid Starvation
glyco ATP Production Rate
mito ATP Production Rate
D
Energetic Map (Basal Rates)
mito ATP Production Rate (pmol/min)
glyco ATP Production Rate (pmol/min)
EV Control
EV Lipid Starvation
ZBTB18 Control
ZBTB18 Lipid Starvation

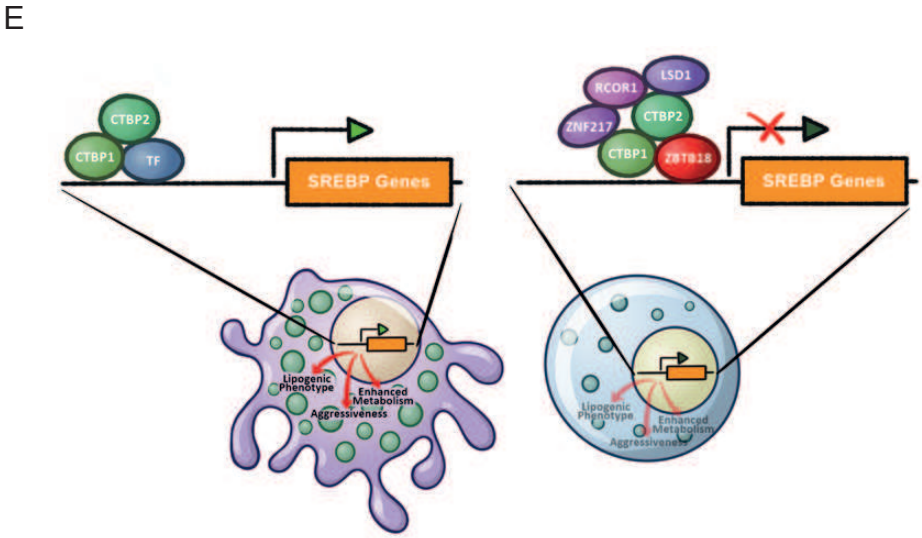
E
CTBP2
CTBP1
TF
SREBP Genes
RCOR1
LSD1
ZNF217
CTBP2
CTBP1
ZBTB18
SREBP Genes
Lipogenic Phenotype
Enhanced Metabolism
Aggressiveness